

**Mechanisms of  
Transformation of  
Bentonite Barriers  
(UMB)**



Gesellschaft für Anlagen-  
und Reaktorsicherheit  
(GRS) gGmbH

## **Mechanisms of Transformation of Bentonite Barriers (UMB)**

Artur Meleshyn

August 2019

### **Remark:**

The underlying work of this report was supported by the Federal Ministry of Economic Affairs and Energy (BMWi) under financial support code 02E11344A.

The work was carried out under the auspices of the Gesellschaft für Anlagen- und Reaktorsicherheit (GRS)gGmbH.

The author is responsible for the content of this report.

**GRS - 390**  
**ISBN 978-3-944161-71-6**

**Key Words**

Bentonite Barriers, Geological Repositories, High-level Radioactive waste, Swelling Gas Pressure

## **Acknowledgement**

The funding by the Federal Ministry of Economic Affairs and Energy (BMWi), represented by the Project Management Agency Karlsruhe (PTKA-WTE), contract no. 02E11344A, is gratefully acknowledged.

Dr. Stephan Kaufhold (BGR, Hannover) is gratefully acknowledged for providing the studied bentonites. The experimental results in this study were obtained owing to a skilful lab assistance of Veronika Prause (preparation of batches, water content, Fe(II)/Fe(III), pH), Uwe Hertes (batch vessels at 120°C, gas pressures, carbonate contents), Michael Kröhn (swelling pressure, permeability), Karin Grupe (solution composition), Felicia Garbe (anion titration, pH, gas analyses), and Sabine Kranz (gas analyses) of the geoscientific laboratory of the GRS. Discussions with Dr. Chun-Liang Zhang (GRS) on experimental design and results are gratefully acknowledged.



## Table of Contents

	<b>Introduction.....</b>	<b>1</b>
<b>2</b>	<b>Materials and Methods .....</b>	<b>7</b>
2.1	Solutions and solids .....	3
2.2	Experimental set-up .....	5
2.2.1	Batches at 25, 60, 90, and 120°C .....	5
2.2.2	Swelling pressure and permeability experiments .....	6
2.3	Measurements .....	9
2.3.1	Carbonate content .....	9
2.3.2	Gas pressure .....	10
2.3.3	Gas sampling and gas analyses .....	10
2.3.4	Solution pH, density, and composition .....	11
2.3.5	Swelling pressure and permeability of compacted bentonites .....	11
2.3.5.1	Force transducers.....	11
2.3.5.2	Fluid injection pressure.....	12
2.3.5.3	Cell corrosion.....	13
<b>3</b>	<b>Results .....</b>	<b>15</b>
3.1	Carbonate dissolution and CO <sub>2</sub> release .....	15
3.1.1	Carbonate contents .....	15
3.1.2	Gas release .....	16
3.2	Changes in solution pH and composition .....	26
3.3	Swelling behaviour.....	32
3.3.1	Effect of microstructural re-organization.....	32
3.3.2	Effect of fluid pressure surges.....	39
<b>4</b>	<b>Concluding remarks .....</b>	<b>43</b>

	<b>Literature .....</b>	<b>49</b>
	<b>List of Tables .....</b>	<b>55</b>
	<b>List of Figures .....</b>	<b>57</b>
<b>A</b>	<b>Annex: Measurements of Fe(III)+Fe(II) and Fe(II) .....</b>	<b>61</b>

# 1 Introduction

Bentonites are considered as barrier materials in geological repositories of high-level radioactive waste in the most disposal concepts worldwide because of their favourable sealing properties. These properties, however, may deteriorate to some extent upon a reaction with aqueous solutions at elevated temperatures. There is no scientific consensus as to which temperatures should be regarded harmless to bentonite performance. According to the last revision of Repository Site Selection Act enacted in Germany in 2017, for example, a provisional temperature limit of 100 °C on the surface of waste containers is to be applied in preliminary safety analyses of geological repositories until higher temperatures are shown to be compatible with performance of geotechnical – often bentonite based – or geological barriers.

In an in-situ study at the Grimsel rock laboratory, a 200-fold increase of CO<sub>2</sub> content to 8.5 vol% in draining pipes inside a highly compacted FEBEX bentonite buffer was unexpectedly observed at 100 °C /JOC 08/. Laboratory experiments with FEBEX bentonite and distilled water at a mass ratio of 1:1 revealed that up to 0.35 and 1 m<sup>3</sup> CO<sub>2</sub> per ton of bentonite were released within 100 days and 10 years at 95 °C, respectively, and the rate of CO<sub>2</sub> release decreased considerably with temperature /JOC 08/. CO<sub>2</sub> was supposed to originate from a reaction between the trapped oxygen and the organics or, alternatively, from a thermal decomposition of the carbonates in bentonite /JOC 08/. Since such non-negligible gas releases from bentonite may result – depending on the available pore volume – in non-negligible or even considerable gas pressures in a geological repository, the present study aimed at gaining more insight into CO<sub>2</sub> release and its origin in bentonites in a series of laboratory experiments. To test the influence of elevated temperatures on both sides of the above-mentioned provisional temperature limit of 100 °C, experiments at 90 °C and 120 °C were carried out as described below.

Swelling pressure and permeability of bentonite-based geotechnical barriers represent key parameters for development of backfilling and sealing concepts of geological repositories of high-level radioactive waste in clay and crystalline formations, as geotechnical barriers must be designed to have a sufficiently low permeability in order to minimise fluid migration across the borders of repository and to achieve safe enclosure of radioactive waste /JOB 17a/, /JOB 17b/. At the disposal depth of several hundred meters, these barriers will experience increase of fluid pressure by several megapascals in the course of establishing hydraulic conditions characteristic of the host formation after the repository closure. Besides, gas production and accumulation in repository may cause

additional fluid pressure increases. In this relation, a concern was raised whether in response to such fluid pressure increases, a hydraulic fracturing of compacted bentonites may occur, which would be accompanied by formation of preferential water infiltration and radionuclide migration pathways through bentonite-based geotechnical barriers or along their interfaces with containers and host rock (or its lining) /KOB 08/, /CHE 16/.

## 2 Materials and Methods

### 2.1 Solutions and solids

Cap rock solution diluted to a salinity of 155 g/l (VGH, from German “verdünnte Gipschlösung”), which is a brine according to a common definition, and a highly saline Opalinus clay porewater (OPA) with a salinity of 19 g/l (Tab. 2.1) were used as model solutions for clay pore waters of Lower Cretaceous and Opalinus clays, respectively, considered as potential host rocks for a geological repository in Germany /JOB 17a/. COX solution used in an auxiliary experiment had a composition (mmol/l): Na<sup>+</sup> (27.7), Ca<sup>2+</sup> (13.3), Mg<sup>2+</sup> (11.0), K<sup>+</sup> (6.82), Sr<sup>2+</sup> (0.06), Cl<sup>-</sup> (31.1), SO<sub>4</sub><sup>2-</sup> (25.0), and HCO<sub>3</sub><sup>-</sup> (0.1). In batches with substrate for stimulation of activity of indigenous microorganisms in bentonites, 0.05 mol/l lactate, 0.05 mol/l acetate, 0.003 mol/l methanol, and 0.0001 mol/l anthraquinone-2,6-disulfonate (AQDS, model substance for humic acid), which was the maximum AQDS concentration soluble in VGH, were added to VGH and OPA.

Bentonites (Tab. 2.2) were provided by Dr. Stephan Kaufhold (BGR, Hannover). Additionally, Opalinus clay (sample “Opalinus BDM\_B9\_19”) and Callovo-Oxfordian (COX) clay (sample “Bure EST 52339”) were provided by Dr. C.-L. Zhang (GRS). Upon delivery, bentonites and clays were pre-crushed in a jaw crusher and ground with Planetary Ball Mill PM 400 (Retsch) for 30 min at 230 rpm using three large (3 cm) and two small (2 cm) balls in the grinding jar. Bentonites, clays and calcite powder (calcium carbonate precipitated p.a., Reag. Ph Eur., ref. no. 102066, Merck) were dried at 50 °C before use. Water content (mass%) of the delivered bentonites is given in Fig. 2.1.

**Tab. 2.1** Chemical composition of VGH and OPA solutions

	VGH		OPA	
	g/l	mol/l	g/l	mol/l
NaCl	145.90	2.497	12.38	0.212
CaCl <sub>2</sub>	3.54	0.032	2.86	0.026
Na <sub>2</sub> SO <sub>4</sub>	5.41	0.038	2.00	0.014
KCl	0.38	0.005	0.12	0.0016
MgCl <sub>2</sub>	–	–	1.61	0.017
SrCl <sub>2</sub>	–	–	0.13	0.0008
NaHCO <sub>3</sub>	–	–	0.04	0.0003
Total	155.24	2.57	19.14	0.27

**Tab. 2.2** Smectite content /KAU 12/ and exchangeable mono- and divalent cation contents /KAU 08/ of studied bentonites

	Origin	Smectite, wt. %	Na+K, meq/ 100 g	Mg+Ca, meq/ 100 g	Delivered bentonites	Ground bentonites
B04	Greece, Milos	91	21	84		
B09	USA, Wyoming	74	63	33		
B10	India, Kutch	89	30	76		
B11	India, Kutch	89	64	51		
B12	India, Kutch	91	57	67		
B13	Hungary	84	3	113		
B16	Germany, Bavaria	70	2	75		
B19	Spain, Almeria	75	23	80		
B23	Argentina	80	69	35		
B31	Armenia	81	52	43		
B36	Slovakia, Liskovec	75	2	53		
B37	Slovakia, Jelsovy Potok	80	2	83		
B38	Russia	63	17	67		
B49	Turkey, Balekesir					
SD80	Greece, Milos					

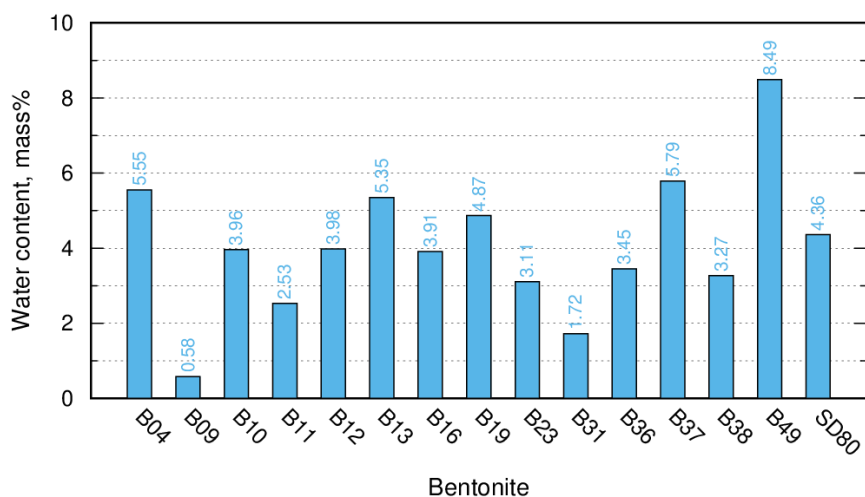


**Fig. 2.1** Water contents (mass%) of unreacted bentonites calculated from the mass difference of the bentonite powder dried at 50 °C for 3 up to 5 days and subsequently at 105 °C for 3 up to 7 days

## 2.2 Experimental set-up

### 2.2.1 Batches at 25, 60, 90, and 120 °C

For time-saving handling, screw cap vessels were chosen first as batch vessels. However, a water loss from them was observed at 90 °C shortly after the start of batches. Sealing the screw caps with a silicon seal, applicable up to 130 °C according to the manufacturer, proved to be effective only for one week at 90 °C. Therefore, all batches at 60 °C and 90 °C were decided to run in welded glass vessels as in /JOC 08/.

For carrying out the first series of batches with 15 bentonites reacting for one year with VGH at 120 °C, welded glass batch vessels were initially used as well. However, five of these batches exploded after several hours of heating in drying oven (Fig. 2.2), and vessels made of Monel alloy 400 (Swagelok) were used henceforth in these batches. 15 alloy vessels with a volume of 150 cm<sup>3</sup> were each filled with 45 g bentonite and 90 g solution, purged with N<sub>2</sub>, gas-tight closed and put on a roll mixer for 35 min to produce bentonite suspensions. These batches had an estimated headspace volume of 46 – 50 cm<sup>3</sup> based on an average bentonite volume of 17.24 cm<sup>3</sup> calculated from the average specific density of 2.61 g/cm<sup>3</sup> of the studied bentonites /KAU 13/ and a solution volume of 82 cm<sup>3</sup> at 25 °C and increasing by 5.5–5.8 % /PHI 81/ to 87 cm<sup>3</sup> at 120 °C. Three vessels containing the suspensions, which had exploded during a heating at 120 °C in welded glass vessels, were equipped for gas pressure monitoring and gas sampling (Fig. 2.2). An additional vessel was used to monitor vapour pressure of VGH solution.



**Fig. 2.2** Left: disrupted and intact welded glass vessels in a drying oven after several hours of heating at 120 °C (inset: a welded glass vessel without aluminium foil). Right: alloy vessels with tubing to pressure transducers outside the oven and a gas sampling valve at the head piece (inset: gas sampling)

In the second series of experiments, 15 g of bentonites B09, B16, B19, and B38 reacted with 30 g of OPA and 32.15 g VGH at 90 °C and 120 °C for 91 up to 166 days in alloy vessels with a volume of 50 cm<sup>3</sup> equipped for gas pressure monitoring. 15 g of B19, in which carbonates were removed according to the sodium acetate – acetic acid method /TRI 86/, reacted with 30 g of OPA at 90 °C. 0.53 g of calcite, which is the major carbonate mineral in the studied bentonites /KAU 12/, reacted with 35.4 g of OPA and 37.90 g VGH at 120 °C. All these batches had an estimated headspace volume of 13.1–13.2 cm<sup>3</sup>. Additionally, 15 g of B19 and B38 reacted with 7.5 and 15 g of OPA at 90 °C for 159 up to 166 days in 50-cm<sup>3</sup> alloy vessels with estimated headspace volumes of 37.0 and 29.8 cm<sup>3</sup>, respectively. In two further batches, 15 g of B19 reacted with 39.0 g and 42.4 g of VGH in 50-cm<sup>3</sup> alloy vessels with estimated headspace volumes of 6.6 and 3.3 cm<sup>3</sup>, respectively. Finally, 15 g of Opalinus clay and 15 g of COX clay reacted with 15 g or 30 g of OPA and COX solution, respectively.

### 2.2.2 Swelling pressure and permeability experiments

To cope with the high number of specimens and a projected prolonged measurement time for the generally low-permeable bentonite material, a bank of initially 12, later extended to 20, specially designed, constant-head, rigid-wall permeameter cells was constructed (Fig. 2.3).

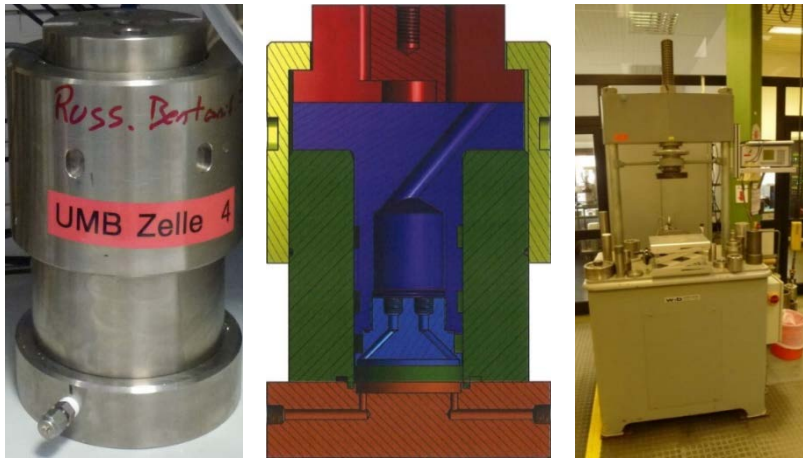


**Fig. 2.3** A permeameter cell used in swelling pressure and permeability measurements (left), a construction drawing showing a vertical section of a permeameter cell (middle), and a hydraulic press used to compact bentonites within permeameter cells (right)

The cells were designed to function as “zero-displacement” cells and to withstand a pressure of 100 MPa, which was identified as the likely maximum combination of solution backpressure and swelling pressure of bentonites in the initial experimental design, and made of titan (10 cells) and stainless steel (10 cells) to resist corrosive attack by high salinity solutions. Bentonite powder after a preliminary drying at 50°C was filled into the cell in between the porous plates and, after installing the load-transfer ram with a force transducer above the top porous plate (Fig. 2.3), was statically compacted to a pellet with a diameter of 5 cm, a height of 1 cm, and a density of 1.6 g/cm<sup>3</sup>. Upon reaching the prescribed height and while the then compacted bentonite remained under the press load, the cap nut was tightened into position without adding axial stress. In the second measurement series, a triple loading/unloading of bentonites was carried out additionally in advance of tightening the cap nut in order to study the effect of mechanical pre-treatment on the swelling pressure evolution. Dry density of compacted bentonites (Fig. 2.4) was calculated from the bulk density of 1.6 g/cm<sup>3</sup> and the water content (Fig. 2.1) according to the relation: dry density = bulk density / (1 + water content).

Compacted bentonite was allowed to absorb solution from a burette connected to the cell from the bottom side (for up to one month, Fig. 2.5) then from the top side (for two to three weeks, Fig. 2.5) to let the trapped air to escape and to approach a saturated state. Swelling of compacted bentonite upon saturation was assumed to seal off possible advective flow pathways along the bentonite-cell interface with solution percolating only through bentonite pores during permeability measurements.

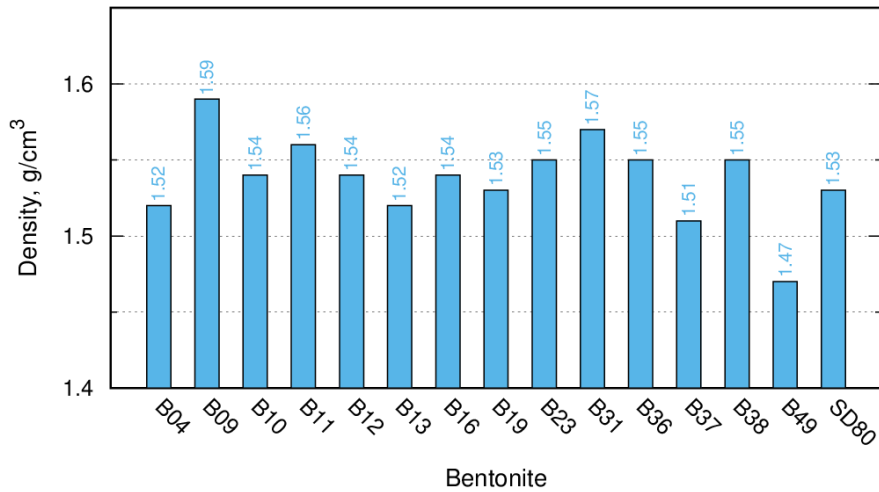


**Fig. 2.4** Dry densities (g/cm<sup>3</sup>) of unreacted compacted bentonites

At swelling pressure equilibrium condition, the fluid pressure at the bottom porous plate was increased from zero to 2 bar and the permeability was calculated from the mass of solution percolating into collecting vessels through tubing connected to the top porous plate in the first and second measurement series (Fig. 2.5). The dynamic viscosity of  $2.084 \pm 0.003 \mu\text{Pa}\cdot\text{s}$  for VGH solution was determined at 25 °C in a series of nine measurements. Swelling pressure measurement was carried out continuously.



**Fig. 2.5** Burettes used to supply VGH to permeameter cells from cell bottoms (left) and cell tops (middle) and by a valve pump to measure the permeability (right, regard plastic vessels connected to cell tops to collect solutions percolating through bentonite pellets)

## 2.3 Measurements

### 2.3.1 Carbonate content

The carbonate content of bentonites was measured according to the method described in /MÜL 71/, /KLO 94/. The home-made carbonate bomb device represents a steel cylinder with a lid screwed on tight by screws with attached pressure transducer (Fig. 2.6). Measurements of CO<sub>2</sub> pressure resulting from the dissolution of inorganic carbonates in 1 g of bentonite powder reacting with 5 ml of 18 % HCl under agitation with a magnetic stir bar were carried out at a lab temperature for up to two hours. Triplicate measurements using three identical carbonate bomb devices were made, and the average value of CO<sub>2</sub> pressure was calculated from the maximum pressures recorded in individual measurements. Calcium carbonate powder was used to calibrate the device by establishing the linear dependence between the mass of the dissolved calcium carbonate and the resulting CO<sub>2</sub> pressure (Fig. 2.7) taking into account the separately measured background pressure due to hydrochloric acid vapour.

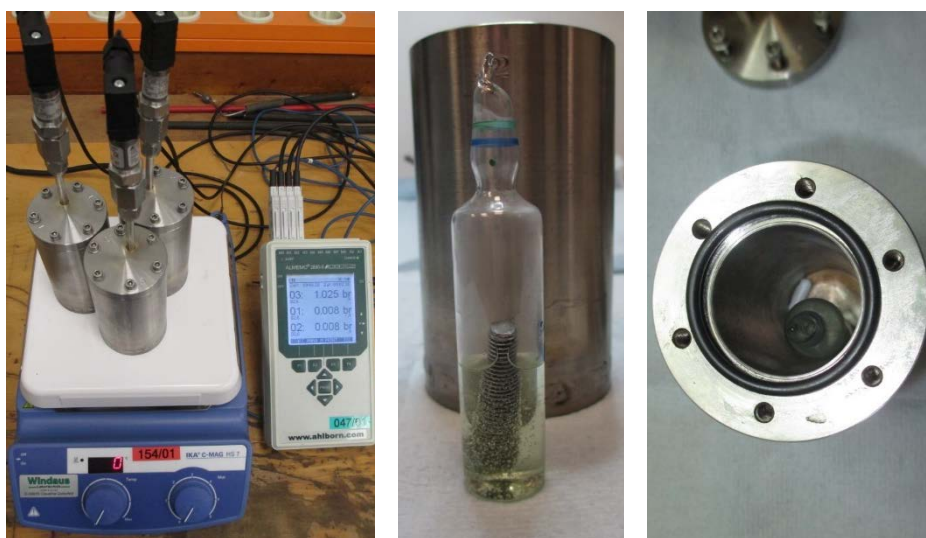


**Fig. 2.6** Home-made carbonate bombs with attached pressure transducers connected to the data acquisition unit (left), a welded glass with 5 ml of 18 % HCl (middle) intended to disrupt upon an agitation after screwing on tight the carbonate bomb lid, and a magnetic stirrer (right) intended to stir the analysed powder material and the acid

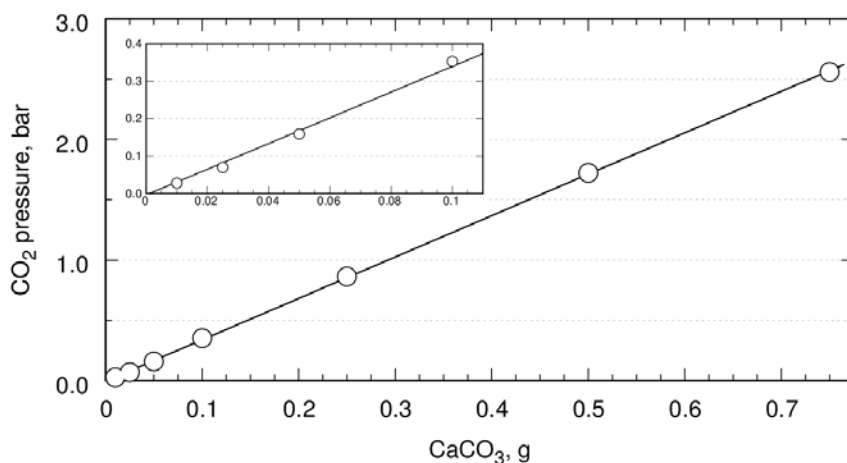


**Fig. 2.7** Average CO<sub>2</sub> pressures as a function of mass of dissolved CaCO<sub>3</sub> obtained from triple (double for 0.75 g CaCO<sub>3</sub>) measurements. Coefficient of determination  $R^2$  for linear regression of data (solid line: pressure =  $(3.43 \pm 0.02) \times \text{mass} - (0.004 \pm 0.006)$ ) equals 1

### 2.3.2 Gas pressure

Gas pressure in the batch vessels and in the carbonate bomb devices was measured by relative and absolute pressure transducers FDA602L4R and FDA602L3A (Ahlborn) with the maximum allowed pressures of 5 and 2.5 bar and the total measurement uncertainty of 0.05 and 0.025 bar, respectively. The pressures measured by the relative pressure transducers were corrected for fluctuations of atmospheric pressure measured using a separate, freely suspended absolute pressure transducer.

### 2.3.3 Gas sampling and gas analyses

Gas sampling was carried out immediately upon taking the vessels out of the oven as shown in the inset in Fig. 2.2. The space between the valve on the head piece of the sampled vessel and the syringe was purged threefold with N<sub>2</sub> before opening the valve and sampling the headspace gas. As soon as smallest droplets of water were noticed to arrive into the syringe, the valve was closed, and the gas sampling was finished. The volume of the sampled gas was read on the syringe scale. The gas analyses were carried out using a gas chromatograph Micro GC 3000 (Inficon) calibrated for measurements in the range of 0.005 – 40 % for CO<sub>2</sub>, 0.0005 – 0.5 % for H<sub>2</sub>, and 5 – 21 % for O<sub>2</sub>.

### **2.3.4 Solution pH, density, and composition**

Decantation of solutions after reaction with bentonites was made using a filter 589/2 (Weißband by Schleicher & Schuell), and the solutions were subsequently filtered by a 0.45 µm filter (Sartorius). pH of solutions was measured using a pH meter by Metrohm subsequently to filtering. pH measurements at the onset (day 0) and after 1, 8, and 30 days of reaction with the studied bentonites at 25°C were carried out in a glove box with Ar atmosphere, whereas those for longer reaction times were made at laboratory conditions. Measurement of Ca, Mg, Na, K, and Si solution concentrations was carried out by ICP-OES iCAP 7400 Duo (Thermo Fisher Scientific). Cl was potentiometrically titrated using titration system Titrando 857 (Metrohm).

### **2.3.5 Swelling pressure and permeability of compacted bentonites**

The first series of measurements was started in September 2016 with then available 12 permeameter cells for 12 bentonites in the initial, air-dry state and VGH solution. The second series of measurements with VGH solution was started in June 2017 with then available 20 permeameter cells for 5 bentonites in the initial, air-dry state (three unreacted bentonites not included in the first series, B10 from the leaked permeameter cell, and B19 in a replicate measurement to prove the result from the first series) and 15 bentonites after a reaction with VGH for one year at 25°C (including two batches with VGH and substrate).

#### **2.3.5.1 Force transducers**

Swelling pressure in permeameter cells was measured by 12 force transducers FKA613 (Ahlborn) and additionally in the second series by 8 force transducers 8402-6020 (burster) with the maximum allowed force of 20 kN. Since the force transducers from burster were smaller than the slots in the permeameter cells, they were fixed in the position using a silicon glue. During the experiment, however, data produced by force transducers from burster differently than data produced by force transducers from Ahlborn showed noticeable fluctuations (Fig. 2.8). An inquiry to burster revealed that the only reason for such fluctuations could have been the application of silicon glue to fix the transducer in the position. Therefore, a technical solution without use of glue should be preferred to fix a force transducer in the position within a permeameter cell.

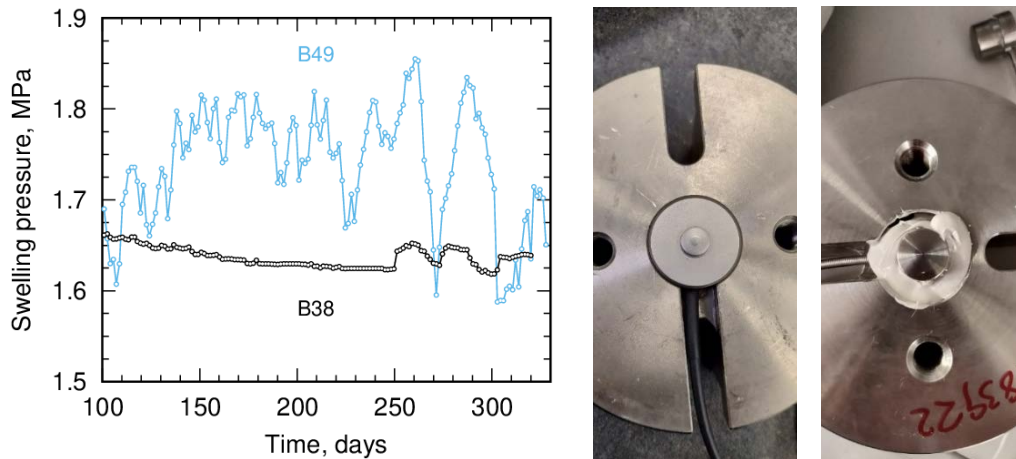


**Fig. 2.8** Swelling pressure evolution (left, MPa) measured by force transducers from Ahlborn (middle, within the cap of the permeameter cell) for B38 and by those from burster (right) for B49

### 2.3.5.2 Fluid injection pressure

Swelling pressure and permeability measurements were carried out at fluid injection pressures of a few bars only instead of the initially planned fluid injection pressures of up to 10 MPa in order to minimize a possibility of hydraulic fracturing compacted bentonites /KOB 08/, /CHE 16/. Since such tests require longer times to accomplish, the thickness of the studied bentonite pellets was set to 1 cm instead of the initially intended 2 cm.

In the first series of measurements, VGH solution was supplied to the cells from burettes at atmospheric pressure (1 bar) during the bentonite saturation phase of the swelling pressure measurement and at a pressure of 2 bar using a pump during the permeability measurement. Although one experiment had to be terminated because of a leak in a measuring cell, the other 11 experiments provided stable permeability values, which indicated the absence of any hydraulic fracturing in the studied bentonite pellets and of bypaths in the measuring cells. On the 79<sup>th</sup> day of the first series of permeameter experiments, an operational malfunction of the piston pump (BESTA HD 2-200) caused an abrupt increase of the fluid injection pressure to 12.6 MPa, which persisted for about 45 min (Fig. 2.9). The pump showed since then further operational irregularities and was replaced by a syringe pump (Teledyne Isco 260D) on the 120<sup>th</sup> day. In the second series, a fluid injection pressure of 0.2 MPa was prescribed, but increased initially to 0.3 MPa upon connecting the permeameter cells to the pump and then on the 86<sup>th</sup> day to 0.44 MPa, decreased below 0.2 MPa on the 90<sup>th</sup> day and below 0.01 MPa on the 170<sup>th</sup> day (Fig. 2.10). The reason for decreases below the prescribed pressure of 0,2 MPa was a salt

crystallization on its mechanical part (following a seal failure), which caused increased mechanical tension apparently misinterpreted by the pump pressure control unit as increased fluid pressure and led to the observed adjustments to lower pressures (Fig. 2.10).

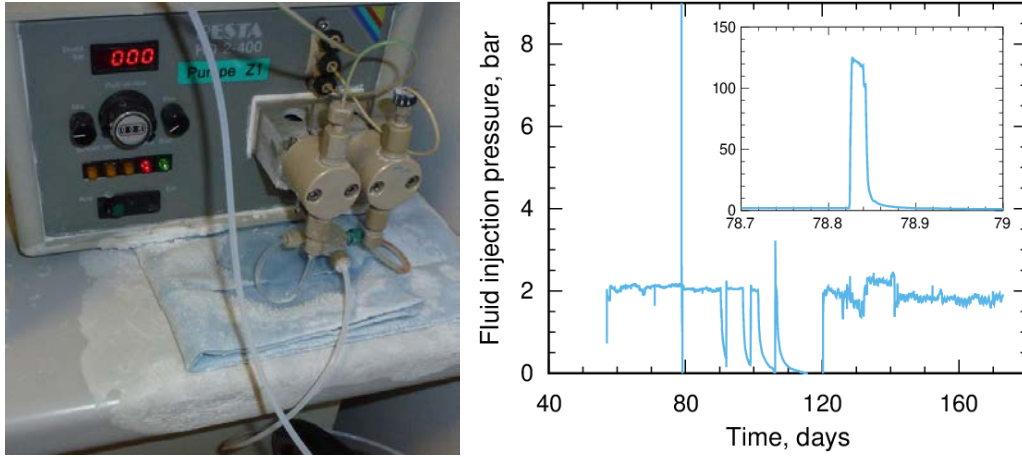


**Fig. 2.9** A solution leak from the piston pump (left) and evolution of the fluid injection pressure (bar) during the first series (right). Inset shows a close-up of the fluid pressure surge

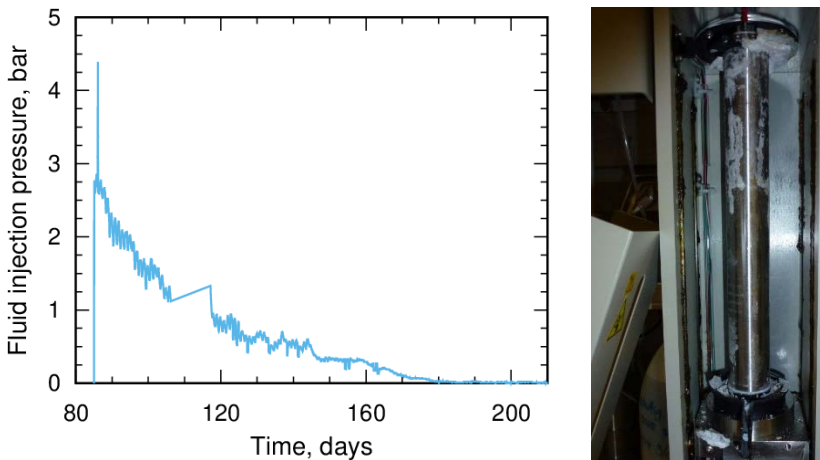


**Fig. 2.10** Evolution of the fluid injection pressure (bar) during the second series (left) and salt encrustations within the syringe pump (right)

### 2.3.5.3 Cell corrosion

For some cells traces of rust were observed as shown in Fig. 2.11, which might be because of use of stainless steel as construction material for several cells. Therefore, a use of cells made of titan for experiments with brines should be preferred.



**Fig. 2.11** Rust traces on the bottom side of unreacted B09 (left) and B23 (middle) pellets and on the porous steel plate in contact with B11 (right, no rust on B11 observed) after permeability measurements

### 3 Results

#### 3.1 Carbonate dissolution and CO<sub>2</sub> release

##### 3.1.1 Carbonate contents

Carbonate contents of the unreacted bentonites vary in the range 0.35 to 9.88 mass% (Tab. 3.1) and agree generally well with those obtained for the studied bentonites earlier from LECO analysis /KAU 12/. Some differences may be attributed to different efficiency of the used methods. In a benchmark with artificial standards /BIR 81/, the carbonate bomb method was found to have a superior precision to the LECO analysis especially for carbonate contents below 10 mass% in sediment samples.

**Tab. 3.1** Carbonate contents (mass%) in unreacted bentonites (/KAU 12/, the present study) and in bentonites reacted with VGH for 374 days at 120 °C, and carbonate loss rate estimate (mass% per year)

	Unreacted /KAU 12/	Unreacted	Reacted	Loss rate
B04	0.0	0.37 ± 0.04	0.00 ± 0.05	≥0.4
B09	2.0	2.35 ± 0.04	1.24 ± 0.12	1.1
B10	1.0	0.62 ± 0.07	0.01 ± 0.13	≥0.6
B11	1.0	1.35 ± 0.10	0.02 ± 0.14	≥1.3
B12	1.0	1.11 ± 0.03	0.00 ± 0.06	≥1.1
B13	4.0	4.65 ± 0.11	2.87 ± 0.08	1.8
B16	0.0	0.44 ± 0.03	0.00 ± 0.08	≥0.4
B19	3.0	3.23 ± 0.05	1.61 ± 0.08	1.6
B23	0.0	0.39 ± 0.03	0.00 ± 0.11	≥0.4
B31	1.0	1.40 ± 0.06	0.30 ± 0.16	1.1
B36	0.0	0.35 ± 0.03	0.00 ± 0.05	≥0.3
B37	1.0	0.39 ± 0.01	0.00 ± 0.04	≥0.4
B38	8.0	9.88 ± 0.13	7.78 ± 0.14	2.1
B49	not measured	3.90 ± 0.05	2.00 ± 0.17	1.9
SD80	not measured	2.80 ± 0.07	1.02 ± 0.12	1.8

A comparison between the values for unreacted bentonites and bentonites reacted at 120 °C (Tab. 3.1) shows that bentonites with initial carbonate contents below ~1.4 mass% lost carbonates completely over a heating period of 374 days. Only a lower boundary of carbonate loss rate can be estimated for these bentonites, as their complete carbonate loss may have occurred well in advance of the experiment termination. The bentonites with initial carbonate contents of  $\geq 1.4$  mass% can be divided into two sub-groups with loss rates of 1.1 (B09, B31) and 1.6–2.1 (B13, B19, B38, B49, SD80) mass% per year upon a reaction with VGH at 120 °C. In additional experiments with B09, B19, and B38 a respective loss of 0.6, 1.7, and 1.4 mass% per year was recorded upon a reaction with VGH at 90 °C, whereas SD80 lost 1.6 mass% per year upon a reaction with OPA at 90 °C. A two-year experiment with B16 and VGH at 25 °C revealed a complete carbonate loss. A similar observation of a complete carbonate loss upon a heating at 200 °C of a Wyoming bentonite with 7 mass% for 1.5 years was made in /YAU 87/. A bentonite with a carbonate content of 20.3 mass% lost up to 7.7 and 15.2 mass% upon a reaction with a groundwater and a distilled water, respectively, at 90 °C for 730 days /FIL 17/.

### 3.1.2 Gas release

The gas pressure in the monitored batch vessels showed a continuous increase until reaching equilibrium values after about 200 to 300 days of reaction except for pressure excursions because of temporary temperature decreases on 5<sup>th</sup>, 53<sup>th</sup> and 61<sup>th</sup> day (putting batch vessels into the oven, a short current interruption) and a pressure decrease for B12 and B31 because of a gas sampling on 138<sup>th</sup> day (Fig. 3.1).

The water vapour pressure of  $1.78 \pm 0.01$  bar observed in our experiment for the VGH solution agrees very well with the value of 1.77 bar reported in the tabulated data for a 2.6 M NaCl solution at 120 °C /FAB 68/. The gas pressure in excess of this vapour pressure after ~130 days of reaction varies for the studied bentonites apparently between ~0.6 and ~1.2 bar. However, the actual excess pressure due to gas release in bentonites in contact with VGH appears to be higher than this estimate as evidenced by gas pressures observed after the gas sampling from the vessels with B12 and B31. During the sampling from the vessel with B31, the headspace pressure decreased from 2.79 bar to 0.26, and within about one day it increased to a value of 1.06 bar, which was maintained for about two days and can be regarded as a proxy for vapour pressure of the solution in contact with B31 at 120 °C. Similar observation was made for bentonite B12, for which the head-

space pressure decreased from 2.95 bar to 0.11 bar during the sampling and increased then within about one day to a value of 1.17 bar, which was maintained for about two days. Thus, the solution in contact with B12 and B31 shows vapour pressures which are lower by 0.61 and 0.72 bar, respectively, than that for the VGH solution.

A first assumption to explain this observation was that the salinity of solutions in contact with bentonites may be higher than that of VGH due to the water uptake in between negatively charged montmorillonite layers, where the negatively charged chloride ions are electrostatically excluded from. This way,  $\text{Na}^+\text{Cl}^-$  ion pairs would remain in a solution with a decreased solvent concentration and a correspondingly increased salinity. To prove this assumption, the vapour pressure of solutions with salinities of 200 and 325 g/l was measured (Tab. 3.2). Upon the salinity increase from 155 g/L for the VGH solution to 325 g/l for the saturated (at 20 °C) cap rock solution, a decrease of water vapour pressure by 0.28 bar was observed, which is considerably smaller than the decreases of 0.61 and 0.72 bar observed for VGH in contact with B12 and B31. It can therefore be assumed that bentonite colloids with cations residing on their negatively charged surface may further decrease the water vapour pressure of the contacting solution in an effect similar to the effect of the dissolved salt. A proof of this assumption is, however, beyond the scope of the present study and shall be addressed in a follow-up study.

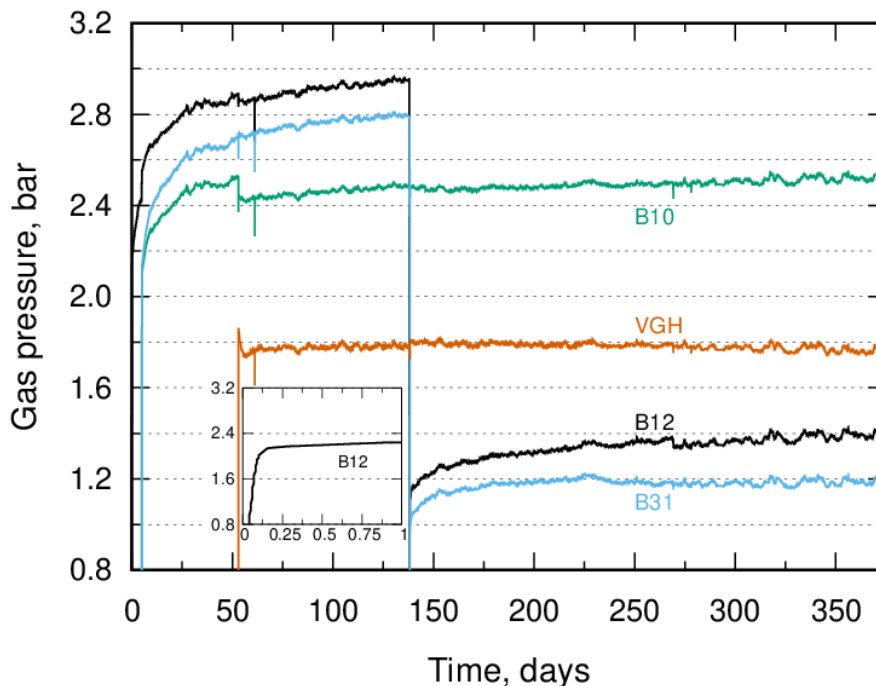


**Fig. 3.1** Gas pressure evolution for 1:2 suspensions of bentonites B10, B12, and B31 with VGH at 120 °C. Inset shows a close-up of the pressure evolution for B12 within the first day of reaction

**Tab. 3.2** Vapour pressures (bar) for OPA and VGH at 90 °C and 120 °C and for diluted (200 g/l) and saturated (325 g/l) cap rock solutions at 120 °C

	OPA, 19 g/l	VGH, 155 g/l	200 g/l	325 g/l
Pressure <sup>*</sup> , 120 °C	1.924 ± 0.003	1.767 ± 0.003	1.674 ± 0.003	1.488 ± 0.001
Pressure <sup>a</sup> , 90 °C	0.657 ± 0.001	0.646 ± 0.001		

<sup>\*</sup>: <sup>a</sup> average values calculated from the data on the last 7 days of a 36-days<sup>a</sup> and a 15-days<sup>\*</sup> experiment

It can be seen from Fig. 3.1 that after the gas sampling the gas pressure in the vessels with bentonites B31 and B12 continued to increase in excess of the tentative vapour pressures of ~1.1 and ~1.2 bar and stabilized eventually at ~1.2 and ~1.4 bar, respectively. Hence, a total excess gas pressure of ~2.0 bar can be estimated for B12 for the whole experiment duration by adding the excess pressures of ~0.2 and ~1.8 bar observed after and before the gas sampling, respectively. Accordingly, an equilibrium gas pressure of ~3.2 bar can be estimated for B12, if no gas sampling were made. As can be seen in the inset of Fig. 3.1, about 65 % (2.07 bar) and 70 % (2.25 bar) of this value were reached within the first three hours and the first day of reaction, respectively. For B31, an excess gas pressure of ~1.1 bar and an equilibrium gas pressure of ~2.3 bar can be estimated in a similar way.

An obvious explanation for the observed excess gas pressures is a gas release from bentonites. Analyses of the headspace gas samples from the batches with B12 and B31 revealed that CO<sub>2</sub> partial volume increased from the initial estimated atmospheric value of ~0.04 vol.% to 24 and 30 vol.% for B12 and B31, respectively.

The second series of experiments provided additional observations on CO<sub>2</sub> release from bentonites. Most importantly, CO<sub>2</sub> release results from a reaction involving not only carbonate minerals but also one or more further bentonite components. This can be concluded from only a minor gas pressure excess of 0.12 – 0.15 bar in the batches with calcite and OPA or VGH as compared to the gas pressure excess of 1.08 –1.17 bar in the batches with B19 despite their similar carbonate contents of 0.5 – 0.53 g (Fig. 3.2 and Fig. 3.3).

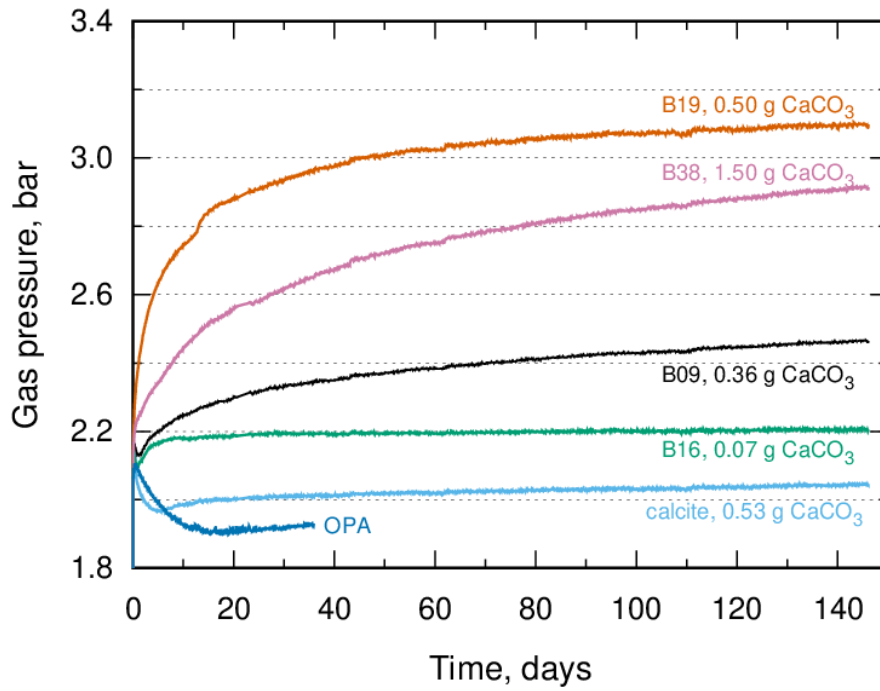


**Fig. 3.2** Gas pressure evolution of 1:2 bentonite suspensions with OPA at 120 °C. The initial mass of CaCO<sub>3</sub> in the batch vessel was calculated from the carbonate contents of unreacted bentonites (Tab. 3.1)

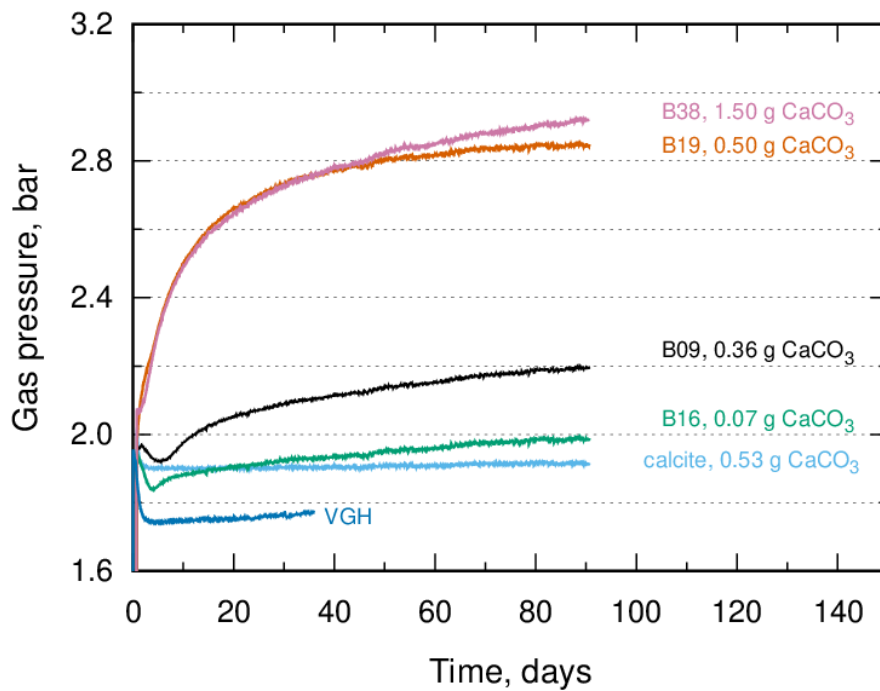


**Fig. 3.3** Gas pressure evolution of 1:2 bentonite suspensions with VGH at 120 °C. The initial mass of CaCO<sub>3</sub> in the batch vessel was calculated from the carbonate contents of unreacted bentonites (Tab. 3.1)

This observation agrees well with the carbonate–clay interaction mechanism /SMI 89/, /HUT 90a/, /HUT 90b/, which is argued to be the ultimate source of abundant CO<sub>2</sub> in most diagenetic environments at temperatures over approximately 7°C /HUT 90a/, /HUT 90b/. This mechanism can be neglected only at temperatures below 50 °C and dominates over a possible precipitation of carbonate minerals above about 100 °C /SMI 89/, /CER 17/. The evolution of CO<sub>2</sub> partial pressure in the range of 0.002 to 130 bar observed across the 10 to 200 °C temperature range with about 400 points from eight sedimentary basins distributed throughout the world was well explained by the assumption of equilibrium between the solutions, carbonate minerals, and various aluminosilicates including one Mg-Al-silicate /COU 98/. The CO<sub>2</sub> partial pressure is buffered by equilibria with these minerals rendering the contribution of CO<sub>2</sub> from organic matter decomposition at elevated temperatures in clays to be considerably smaller than that from the dissolution of carbonates /HUT 90a/, /HUT 90b/, /CER 17/, /COU 98/.

The contribution of CO<sub>2</sub> from organics in the studied bentonites can be assumed negligible also considering that the organics content is below 0.1 mass% for bentonites B12, B19, and B31; equals to 0.1 mass% for B9, B10, and B16 and to 0.3 mass% for B38 /KAU 08/. Taking into account that CO<sub>2</sub> makes up to 10 mass% of the kerogen in clay /BRU 12/ and that CO<sub>2</sub>, which is released at temperatures below 200°C, contributes, e.g., for Boom clay up to 5.5 mass% of the kerogen /LOR 08/, /BRU 12/, the mass of CO<sub>2</sub> to be released from a bentonite with 0.3 mass% of organics at the experimental conditions of this study would not exceed 0.17 mg per g clay. For comparison, the mass of CO<sub>2</sub> to be released from a bentonite with 0.3 mass% of calcite due to its dissolution equals to 1.8 mg per g clay.

Measured gas compositions confirmed that the gas pressure excess is due to CO<sub>2</sub>, which contributed in average 30.9 to 37.8 vol.% followed by H<sub>2</sub> (0.4 to 1.5 vol.%), O<sub>2</sub> (1.0 to 1.1 vol.%), and trace amounts of carbohydrates with the remainder being N<sub>2</sub>. CO<sub>2</sub> head-space contents (Tab. 3.3), determined from the measured gas compositions and sampled gas volumes, agree very well with the observed final proportions between the CO<sub>2</sub> pressures in Fig. 3.2 and Fig. 3.3. The data on H<sub>2</sub>, which most probably originated from the corrosion of the alloy vessels /SCH 12/, indicates that more saline VGH is more corrosive than OPA and that there might be a strong dependence of the corrosion kinetics on the bentonite identity with, e.g., B09 inducing an order of magnitude higher headspace H<sub>2</sub> content (an indication of corrosion extent) in suspension with OPA than do B16 and B38 (Tab. 3.3). This data indicates further that the gas pressure excess of 0.12 – 0.15 bar in the batches with calcite, which was

discussed above, is mainly due to the partial pressure of H<sub>2</sub>.

Second important observation is that CO<sub>2</sub> release from different bentonites does not linearly depend on their initial carbonate content at least within the observation period of up to five months, as bentonite B38 shows comparable or lower gas pressure and head-space CO<sub>2</sub> content than does B19 (Fig. 3.2, Fig. 3.3, Tab. 3.3) while having a threefold initial carbonate content (Tab. 3.1). This observation suggests, e.g., that discarding mainly carbonate origin of CO<sub>2</sub> releases of up to 3.2 l per kg clay and day at 200 °C on grounds of the absent correlation to carbonate contents in /HOM 03/ might have not been justified. Considering further that gas pressure and headspace CO<sub>2</sub> content are not higher for B38 than for B19 despite the higher carbonate loss rate for B38 than for B19 (Tab. 3.1), it ought to be assumed that a part of the dissolved carbonates or released CO<sub>2</sub> in B38 may be bound in a reaction with some bentonite component(s).

Third observation is that carbonate dissolution depends on both solution composition and bentonite identity, as upon 91 days of reaction with OPA bentonites B09, B16, and B19 show a gas pressure higher by 0.1–0.2 bar than upon 91 days reaction with VGH, whereas B38 shows a pressure change of 0.1 bar in the opposite direction (Fig. 3.2, Fig. 3.3). The experiments at 90 °C point up this observation, since OPA dissolves more carbonates than does VGH in B19 and vice versa in B38 (compare data for the solid-liquid ratio of 1:2 in Fig. 3.4 and Fig. 3.5).

**Tab. 3.3** Headspace CO<sub>2</sub> and H<sub>2</sub> contents (ml) of bentonite and calcite suspensions with VGH and OPA after 91 and 146 days of reaction at 120 °C, respectively

	CO <sub>2</sub>		H <sub>2</sub> <sup>a</sup>	
	VGH	OPA	VGH	OPA
B09	4.1	5.5	0.30	0.07
B16	1.5	2.3	0.01	0.007
B19	9.4	9.0	0.76	0.21
B38	10.5	7.0	0.19	0.005
calcite	— <sup>*</sup>	0.16	0.35	0.24

<sup>\*</sup> a value of 4.1 ml was measured, which was discarded as an obvious outlier

<sup>a</sup> the values for B16+VGH/OPA and B09/B38+OPA were within the calibrated range of H<sub>2</sub> contents below 0.5%, whereas the other values can be regarded only as an indication of the gas release trend

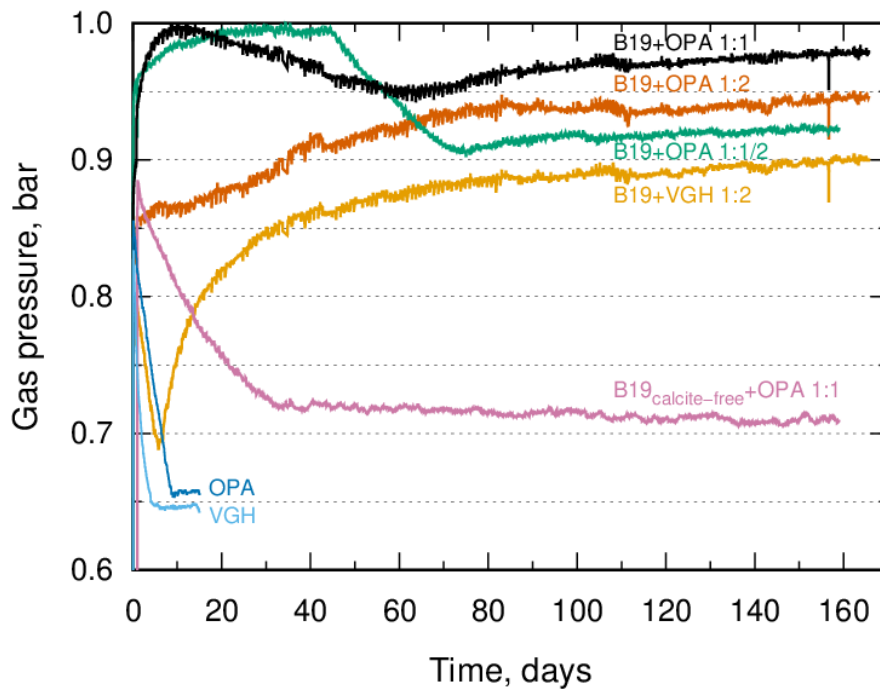


**Fig. 3.4** Gas pressure evolution of 1:2, 1:1, and 1:1/2 suspensions of bentonite B19 with OPA and VGH at 90 °C

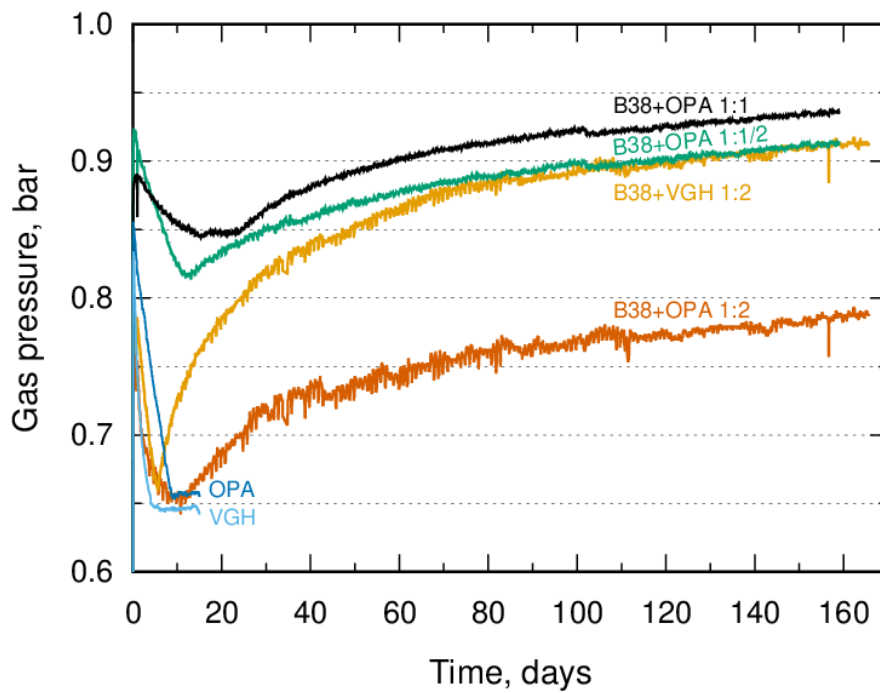


**Fig. 3.5** Gas pressure evolution of 1:2, 1:1, and 1:1/2 suspensions of bentonite B38 with OPA and VGH at 90 °C

The experiments at 90 °C reveal further that carbonate dissolution at this temperature is characterized by gas pressures of up to 1 bar, which are lower by about three times than those at 120 °C and agree very well with the CO<sub>2</sub> pressure of about 1 bar observed in an in-situ experiment in Callovo-Oxfordian clay in the underground research laboratory at Bure (France) due to calcite dissolution at 85 °C /NEC 16/. A decrease in gas pressure at 90 °C as compared to 120 °C can be attributed to a decreasing with temperature rate of CO<sub>2</sub> release as observed for 1:1 suspension of FEBEX bentonite and distilled water at 20, 50, and 95 °C /JOC 08/. A similar conclusion can be drawn from a comparison of the CO<sub>2</sub> release rates of up to 3.5 cm<sup>3</sup> per kg bentonite and day observed in the latter study at 95 °C and up to 3200 cm<sup>3</sup> per kg clay and day at 200 °C in /HOM 03/.

A batch with a B19 sample, in which carbonates should have been removed by sodium acetate – acetic acid method, confirms that the gas pressure in excess of vapour pressure of VGH and OPA solutions originates primarily, if not completely, from carbonates (Fig. 3.4). Yet, the gas pressure in this batch was higher than the OPA vapour pressure, and the headspace still contained 0.72 ml of CO<sub>2</sub> (along with 0.23 ml of H<sub>2</sub> which compare well with the value of 0.21 ml of H<sub>2</sub> at 120 °C in Tab. 3.3), which indicates that either the removal of carbonates in the studied sample was not complete or some CO<sub>2</sub> might originate from another source than carbonate dissolution.

From the experiments at 90 °C, a fourth observation can be made that a decrease of the bentonite-solution mass ratio can result in an increase of the gas pressure excess. This is most clearly evidenced by an increase of the gas pressure excess in 1:1 suspensions of B38 (and, less significant, of B19) as compared to 1:2 suspensions despite a related more than twofold increase of the headspace volume (Fig. 3.4 and Fig. 3.5). A further decrease of the solid-solution ratio to 1:1/2 accompanied by a further increase of the headspace volume leads, however, to a decrease of the gas pressure excess.

Fig. 3.6 shows further for the experiments at 120°C that a moderate increase of the bentonite-solution mass ratio accompanied by a decrease of the headspace volume may result either in an increase or in a decrease of the gas pressure excess.

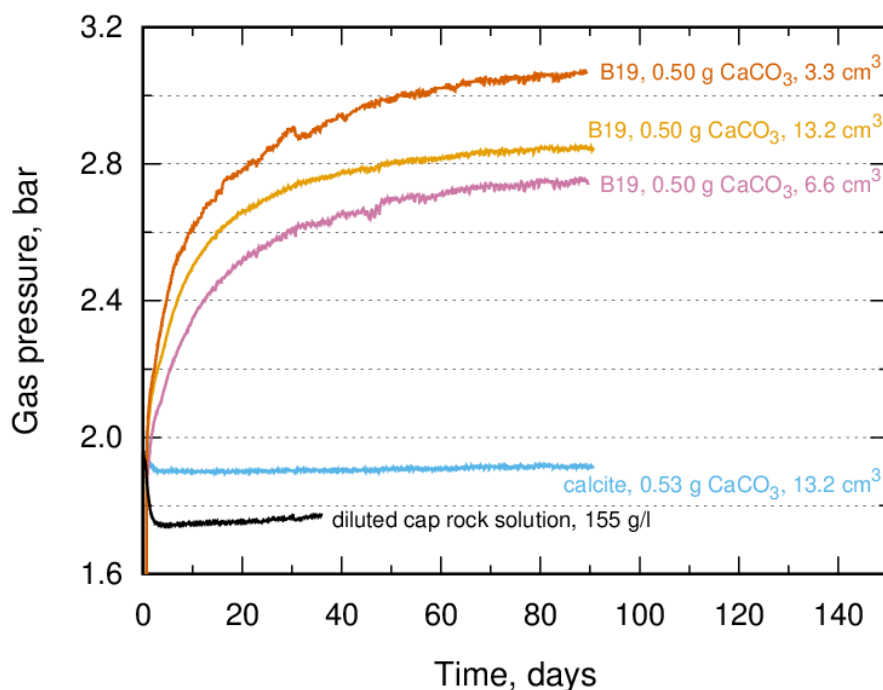


**Fig. 3.6** Gas pressure evolution of bentonite suspensions with VGH at  $120.33 \pm 0.04^\circ\text{C}$ . Headspace volume in the vessels with suspensions was adjusted to 3.3, 6.6 and  $13.2 \text{ cm}^3$  by varying the VGH volume

Dissolution of carbonate minerals according to the carbonate–clay interaction mechanism is proposed to be driven either by silicate hydrolysis or by acids produced from organics in a thermal recovery process /HUT 90a/. Concerning the silicate hydrolysis, it is hypothesized in /HUT 90b/ that as temperature increases, silicates tend to coexist with fluids requiring higher hydrogen ion activity at a given salinity, leading to dissolution of calcite according to the reaction  $\text{CaCO}_{3(s)} + 2\text{H}^+ \rightleftharpoons \text{Ca}^{2+} + \text{CO}_{2(aq)} + \text{H}_2\text{O}$ . This reaction is responsible for the buffering capacity of bentonites, which maintains the pH of porewater in circumneutral or slight alkaline to alkaline range. The reaction equation indicates, however, that upon a sufficiently high increase of  $\text{CO}_2$  partial pressure, the calcite dissolution can be inhibited and, accordingly, the buffering capacity of bentonites can be cancelled.

Exactly that was observed in the in-situ experiment in the URL Bure (France) upon an increase of  $\text{CO}_2$  partial pressure to about 1 bar as a result of carbonate dissolution in clay at  $85^\circ\text{C}$  /NEC 16/. Following that, pH of the solution in contact with clay decreased within 200 days from the initial value of 7.2 to 4.5 because of the oxidation of accessory pyrite in clay. Since the corrosion rate of metallic waste containers increases considerably at acidic pH, precautions should be taken in disposal concept utilizing clays to prevent

such pH drops (as actually made upon this observation in the French disposal concept /NEC 16/).

Batches at 90 °C with samples of COX and Opalinus claystones consisting to, respectively,  $53.6 \pm 0.6$  mass% and  $15.2 \pm 0.2$  mass% of carbonates, show that similarly to the second observation discussed above for bentonites, CO<sub>2</sub> release from claystones does not linearly depend on their initial carbonate content at least within the observation period of about five months, as COX clay shows lower gas pressure (Fig. 3.7) and headspace CO<sub>2</sub> content (1.5 ml) than does Opalinus clay (2.0 ml) while having a more than threefold initial carbonate content. Interestingly too, the headspace of 1:2, 1:1/2, and 1:1 suspensions of B19 at 90°C contained 0.20–0.23 ml of H<sub>2</sub>, whereas for claystones only 0.0014 ml (COX) to 0.0079 ml (Opalinus) of H<sub>2</sub> were measured after about 5 months under otherwise identical conditions. This observation, if confirmed, would mean that bentonites may either facilitate corrosion of the alloy vessels or represent a source of H<sub>2</sub>.

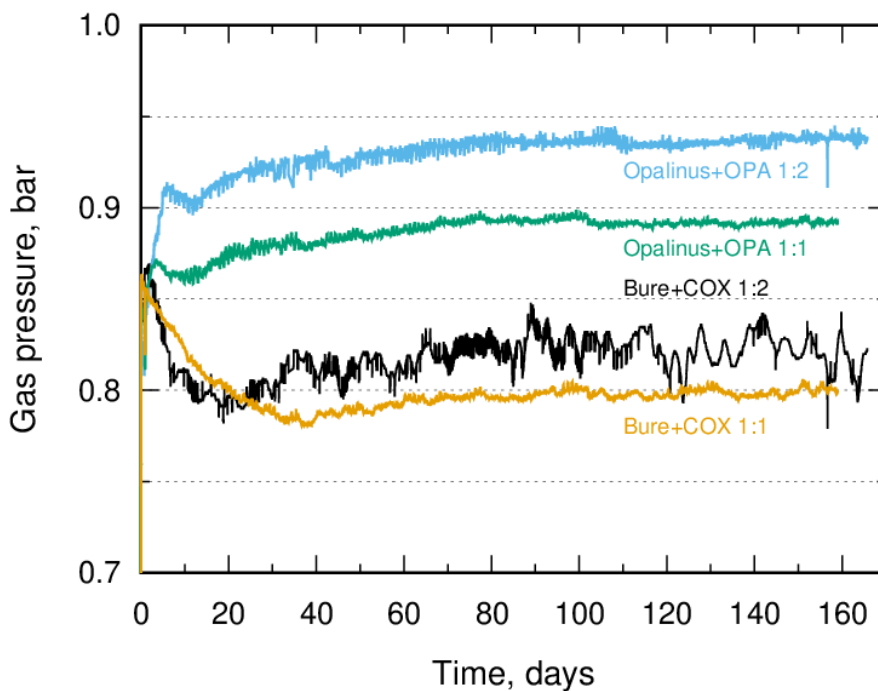


**Fig. 3.7** Gas pressure evolution of Opalinus and COX (Bure) claystone 1:1 and 1:2 suspensions with OPA and COX at  $90.5 \pm 0.2$ °C. Headspace volume of the vessels was adjusted to 13.2 cm<sup>3</sup>

### 3.2 Changes in solution pH and composition

pH of the pore solution in a compacted bentonite conditions is an important parameter for performance assessment because of its influence on radionuclide solubility and sorption. The main buffering reactions are provided by calcite equilibrium and proton exchange reactions occurring at the clay edge sites /WER 03/, /BRA 02/. The average pH value of  $7.25 \pm 0.14$  was calculated for all bentonites except B04 and B37 after 760 days of reaction with VGH at 25°C (Fig. 3.8), which coincides with the pH of 7.25 of the VGH solution before mixing with bentonites. For B04 and B37, pH decreases observed within the first 30 days of reaction are comparable with those which occurred in the aftermath, and the final pH values are well below 5. While pH for B36 was below 5 within the first 30 days of the reaction, it reached a near neutral pH range at the latest after 430 days of reaction. During this period of observation, OPA solution in contact with B36 had a pH which was  $0.58 \pm 0.08$  pH units higher than that for VGH solution. This difference corresponds very well to that of 0.56 pH units between the pH of 7.25 for VGH and 7.81 for OPA measured before mixing with bentonites. These results suggest that reaction times of at least one to two years may be necessary for a realistic estimation of equilibrium pH values of bentonite suspensions.

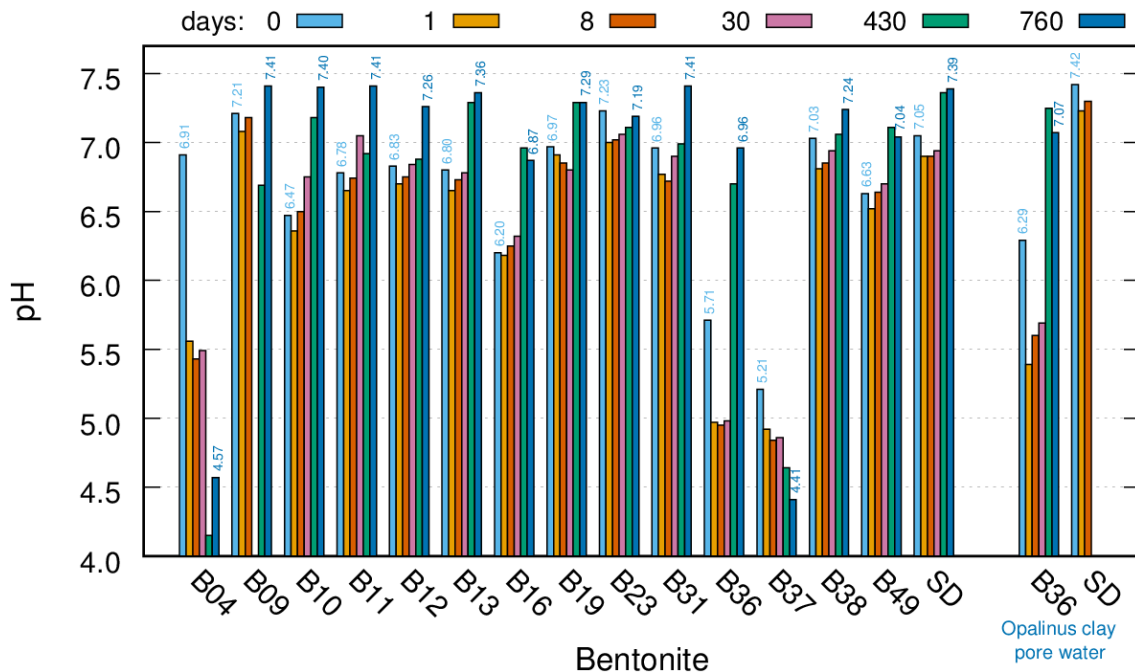


**Fig. 3.8** pH of VGH and OPA at the onset and after 1, 8, 30, 430 ± 11, and 760 days of reaction with bentonites at 25°C. Low volumes of supernatant OPA for SD80 precluded pH measurements after 8 days of reaction

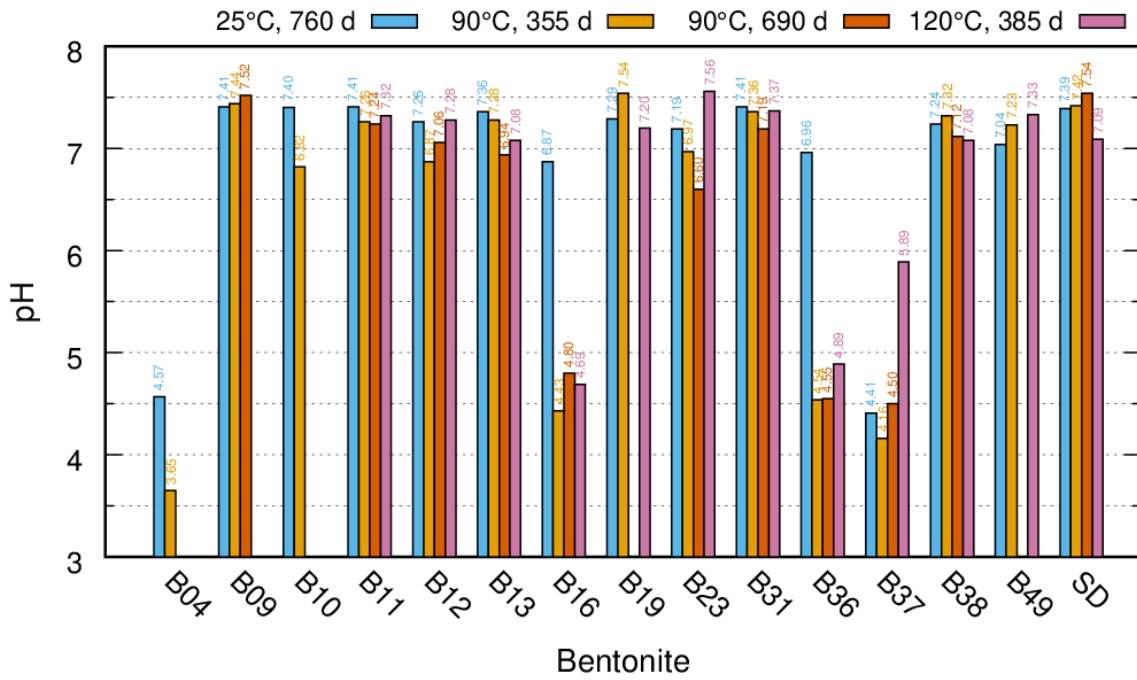


**Fig. 3.9** pH of VGH after reaction with bentonites for 760 days at 25°C, 355 ± 5 days at 90°C, 690 days at 90°C, and 385 days at 120°C

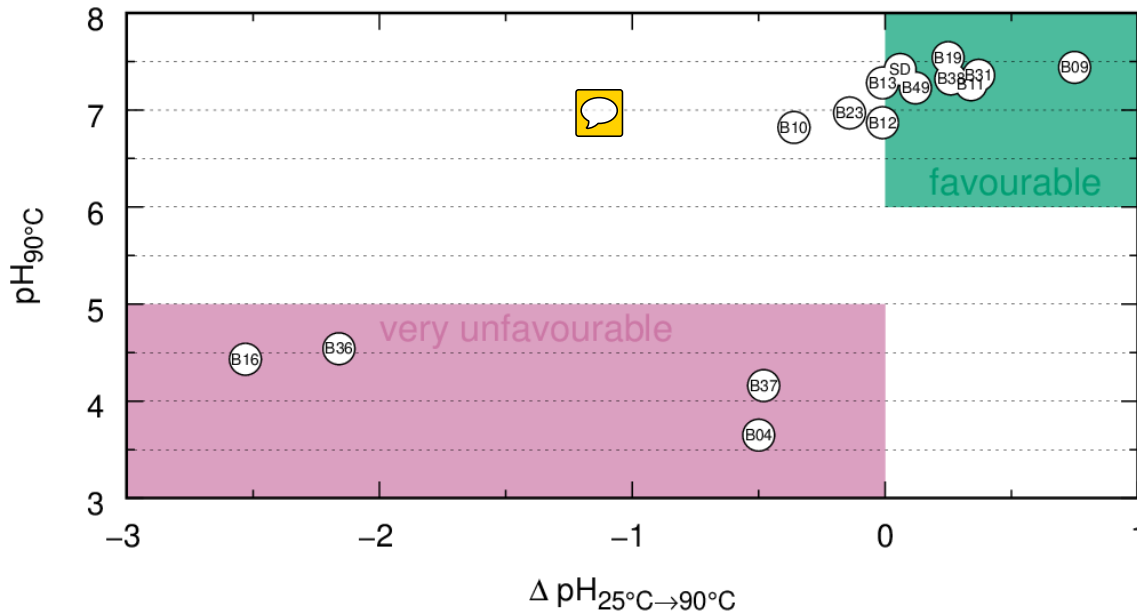


**Fig. 3.10** pH of VGH after reaction with bentonites at 90°C for 355 days plotted against the pH differences between VGH solutions after reaction with bentonites at 25°C for 760 days and at 90°C for 355 days

Data for 90 °C and 120 °C (Fig. 3.9) reveals that pH for B16 and B36 also decreased below 5 after one year of reaction. Fig. 3.10 illustrates that pH values for B04, B16, B36, and B37 showed the strongest decreases upon temperature increase from 25 °C to at

90 °C and declined into acid range, which is very unfavourable concerning the corrosion of metallic components in a repository.

A comparison between VGH and OPA with and without addition of substrate for stimulation of activity of indigenous microorganisms in B36 (Tab. 3.4) shows that at temperatures relevant for microbial activity no clear effect of the latter could be discerned, since while the absolute pH differences after two years of reaction do not exceed 0.23 pH units for VGH and 0.57 pH units for OPA, the sign of pH difference at 60 °C is opposite to those at 25 and 90 °C.

As discussed above, the dissolution of carbonates may be driven by silicate hydrolysis, due to which the contacting solutions would tend to lower pH at higher temperatures /HUT 90a/, /HUT 90b/. Fig. 3.11 and Fig. 3.12a show that there might be some relation between pH, Si concentration, and temperature, as for both one-year and two-year batches with bentonites B16 (without substrate) and B36 (with and without substrate) pH strongly decreased and Si concentration strongly increased upon an increase of temperature from 25 °C to 90 °C. However, no comparably strong decreases occurred for the other bentonites despite the observed strong increases of Si concentration with temperature. Furthermore, Si concentrations at 120 °C decreased to some extent compared to those at 90°C. Therefore, the obtained data does not allow obtaining more insight into the putative mechanism of carbonate dissolution in the studied bentonites.

**Tab. 3.4** pH of VGH and OPA after reaction with B36 for one and two years at 25, 60, and 90°C with (denoted by “μ”) and without substrate addition

	VGH		OPA	
	1 year	2 years	1 year	2 years
25°C	6.70	6.96	7.25	7.07
25°C, μ	7.50	7.16	6.90	7.50
60°C	6.10	5.88	6.95	6.36
60°C, μ	5.56	5.55	7.03	5.79
90°C	4.54	4.55	5.11	5.02
90°C, μ	4.74	4.76	5.23	5.15

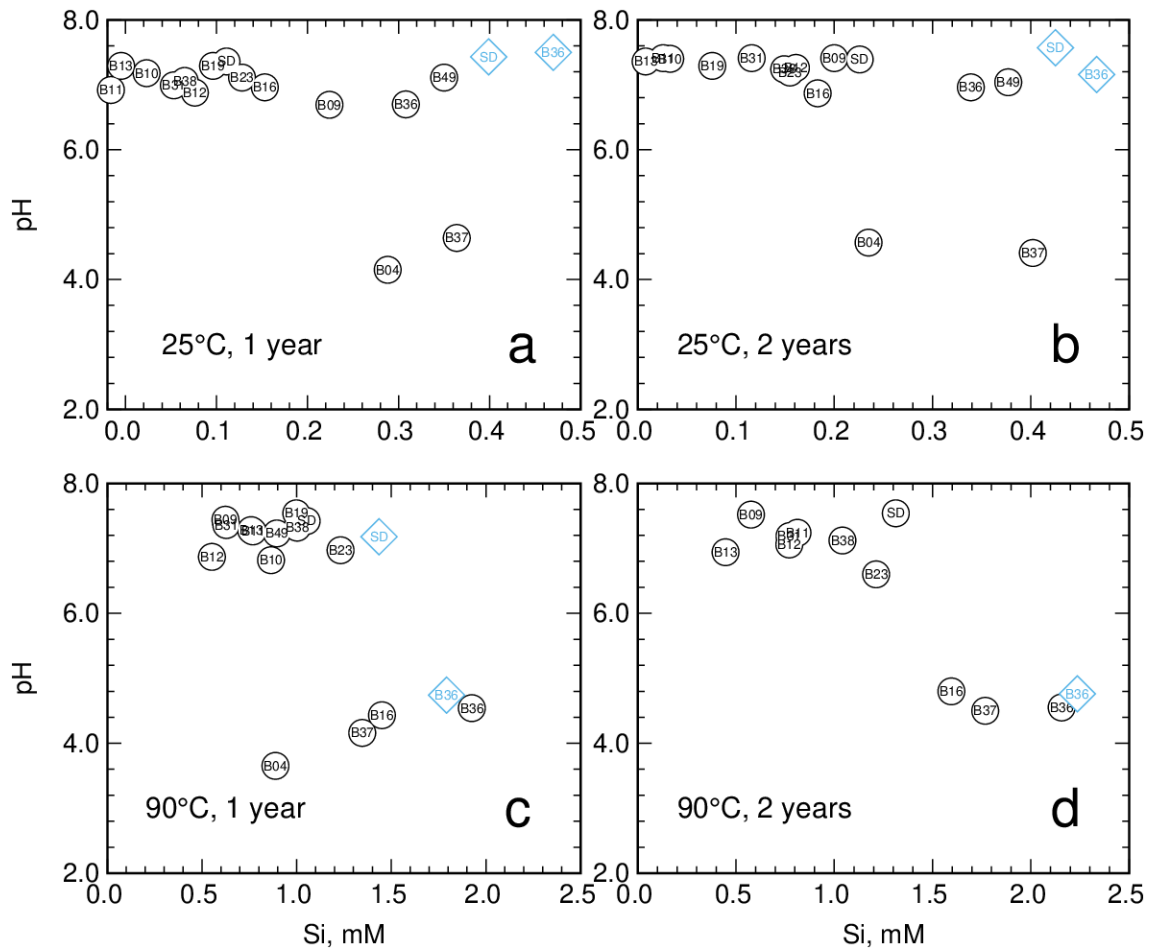


**Fig. 3.11** pH plotted against Si concentration (mM) for VGH without (circles) and with substrate (diamonds) after one- and two-year reactions with bentonites at 25 and 90°C

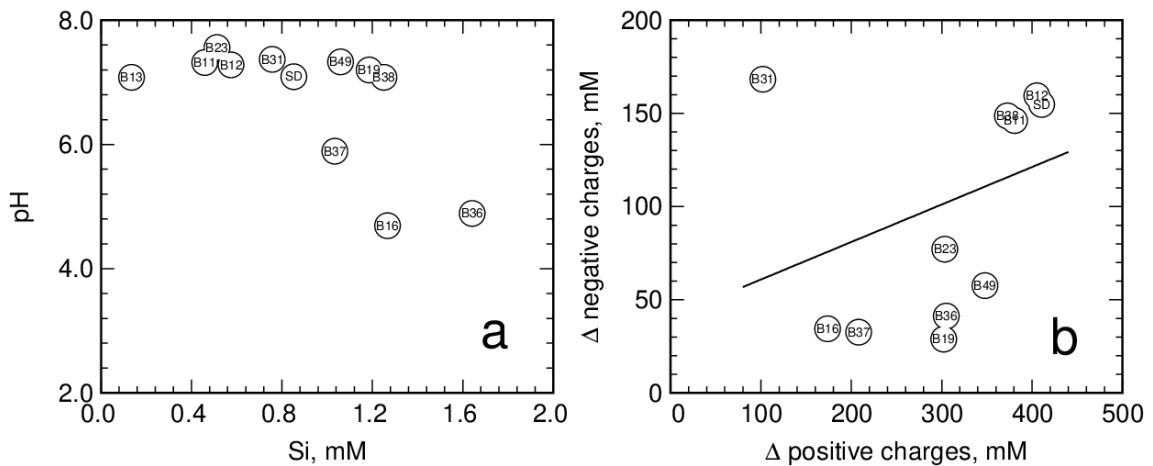


**Fig. 3.12** (a) pH plotted against Si concentration for VGH after one-year reaction with bentonites at 120°C, and (b) corresponding shifts of charge concentrations. Coefficient of determination  $R^2$  for linear regression of data in graph b ( $\Delta n.c. = (0.20 \pm 0.11) \times \Delta p.c. + 41 \pm 24$ ) equals 0.20

As suggested in the discussion to Fig. 3.1 concerning the decreased water vapour pressure of VGH, ionic concentrations of a solution would increase upon its contact with unsaturated clay because of a selective water uptake into the interlayer spaces between negatively charged smectite sheets, where anions are electrostatically excluded from and remain in the solution along with accompanying cations. Alongside with this,  $\text{Na}^+$  from VGH would partially exchange interlayer  $\text{Ca}^{2+}$ ,  $\text{Mg}^{2+}$ , and  $\text{K}^+$ , whereas additional  $\text{Ca}^{2+}$  would predominantly, if not completely, come from the dissolution of carbonates as discussed above.

Fig. 3.12b and Fig. 3.13 show that charge concentrations calculated for VGH suspensions at 25, 90, and 120°C from the measured  $\text{Na}^+$ ,  $\text{Ca}^{2+}$ ,  $\text{Mg}^{2+}$ ,  $\text{K}^+$ ,  $\text{Cl}^-$ , and  $\text{SO}_4^{2-}$  concentrations indeed strongly increase upon a reaction of VGH with bentonites. The presence of correlation for three datasets (graphs a, c, and d in Fig. 3.13) support the suggestion that a selective water uptake from the solution into the interlayer spaces of contacting bentonites may take place. However, the datasets for two-year-reaction at 25°C and one-year-reaction at 120°C do not show such a correlation, therefore, no unequivocal conclusion can be made with respect to the mechanism of changes of ionic concentrations in studied suspensions.

Regression equations for this data reveal further that measured concentrations of positive charges expectedly outbalance those of negative charges, as important anionic components  $\text{HCO}_3^-$  and  $\text{CO}_3^{2-}$  were not measured for the studied solutions. Assuming that these two anions would compensate the excess positive charge in the solution, increase of their concentration upon reaction of VGH (without substrate) with bentonites can be estimated to vary in the ranges of 100 to 235 mM for one-year reaction at 25°C, 52 (except for the only lower value of -22) to 396 mM for two-year reaction at 25°C, 273 to 459 mM for one-year reaction at 90°C, 23 to 265 mM for two-year reaction at 90°C, and 139 (except for the only lower value of -66) to 290 mM for one-year reaction at 120°C.

These ranges are comparable, although in the case of two experimental series at 90°C they do not intercept and, most interestingly, the estimated concentration of putative  $\text{HCO}_3^-$  and  $\text{CO}_3^{2-}$  for the two-year series is lower than for the one-year series. Considering that as discussed above the extent of carbonate dissolution, which can be assumed to be a source of these anions, within two years should not be lower than within one year under otherwise identical conditions, this observation might suggest that a part of the dissolved carbonates or released  $\text{CO}_2$  may be bound in a reaction with some bentonite component(s).

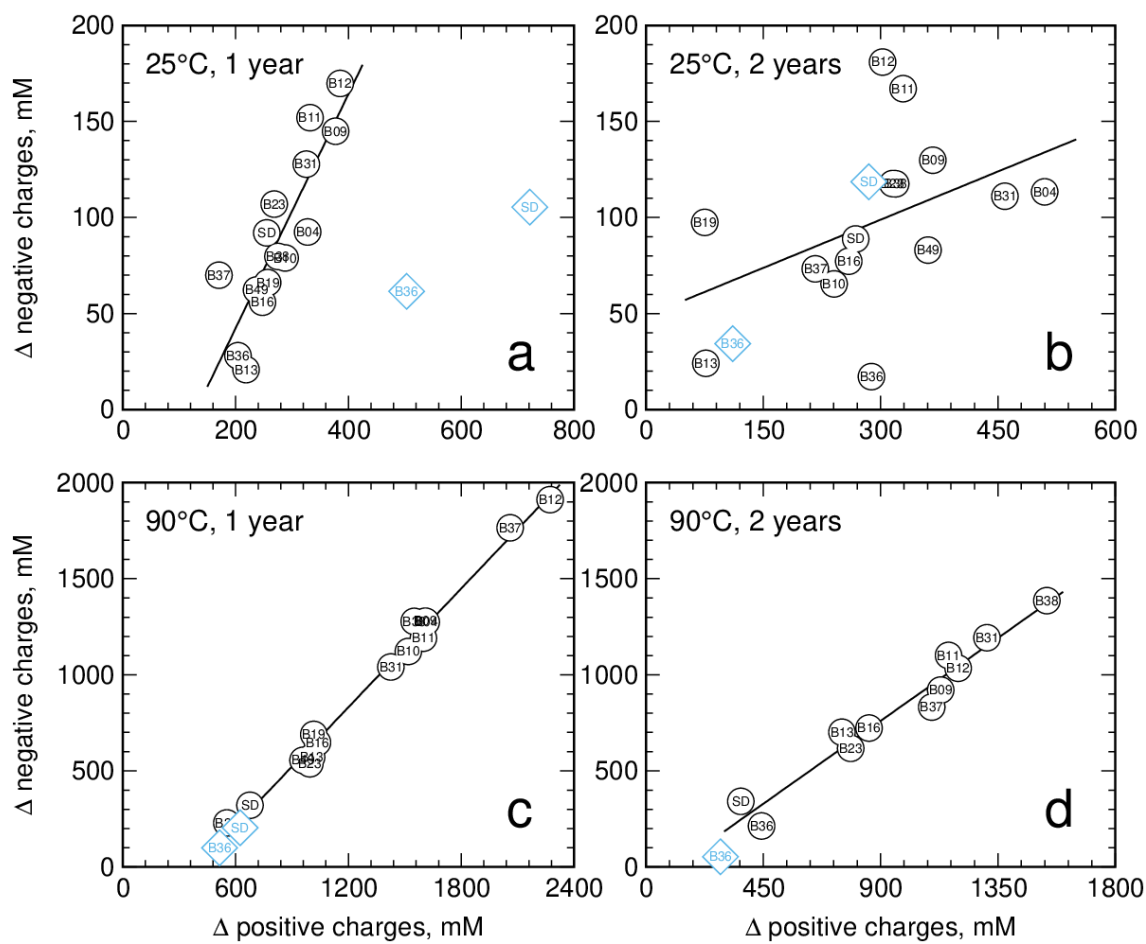


**Fig. 3.13** Shifts of charge concentrations in VGH without (circles) and with substrate (diamonds) relative to unreacted VGH after one- and two-year reactions with bentonites at 25 and 90 °C

Coefficient of determination  $R^2$  for linear regressions of data in graphs a, b, c, and d ( $\Delta n.c. = 0.6 \times \Delta p.c. - 79$ ,  $\Delta n.c. = 0.17 \times \Delta p.c. - 49$ ,  $\Delta n.c. = 1.03 \times \Delta p.c. - 404$ , and  $\Delta n.c. = 0.96 \times \Delta p.c. - 102$ ) equals 0.74, 0.25, 0.99, and 0.95, respectively

Even though carbonates present in the studied bentonites should dissolve at the applied experimental conditions as discussed in the previous section, a precipitation of some carbonate mineral with a composition stable at 90°C after one year of reaction might not be excluded either. However, this appears not to be a dominating reaction considering the discussion to Fig. 3.2, Fig. 3.3, Tab. 3.1 and Tab. 3.3 in the previous section that gas pressure and headspace  $CO_2$  content are not higher for B38 than for B19 despite the higher carbonate loss rate for B38 than for B19. Since a precipitation of some carbonate mineral would counteract the loss of carbonates, which was however not measured, it ought to be concluded that a reaction of the dissolved carbonates or released  $CO_2$  with some bentonite component(s) may be dominating.

It is noticeable that in one-year series at 25°C the disbalance between measured positive and negative charges for VGH with substrate is much stronger than that for VGH without substrate and does not match the correlation observed for the latter, which might be a manifestation of a microbial effect on the solution composition. It is, however, not clear from the available data, why this observation does not persist for the two-year series at 25°C, and more broadly, why the correlation observed for VGH without substrate for the one-year series at 25°C does not persist for the two-year series at 25°C.

### **3.3 Swelling behaviour and permeabilities**

#### **3.3.1 Swelling pressure and permeability**

For bentonites from Skalna, Holmehus, Rösna, Friedland, Milos, and Wyoming compacted to dry densities of 1.54–1.60 g/cm<sup>3</sup>, swelling pressures in the range 0.85–5.4 MPa were observed upon saturation with 3 M NaCl solution /KAR 06/. For comparison, swelling pressures in the range 1.4 – 7.6 MPa were observed for these bentonites upon saturation with de-ionized water /KAR 06/. Swelling pressures of 2.8 MPa and 2.9 – 3.1 MPa were observed for FEBEX bentonite saturated with a 2.5 M NaCl solution at a dry density of 1.65 g/cm<sup>3</sup> /LLO 07/ and for GMZ01 bentonite saturated with a 2 M NaCl solution at a dry density of 1.70 g/cm<sup>3</sup> /ZHU 13/, /CHE 15/, respectively. Swelling pressures observed for unreacted bentonites in the present study, except for B12, B23, and B37, compare well with the values reported in the literature for brines as saturating medium (Tab. 3.5).

Laboratory and in situ permeabilities of argillaceous rocks were found to vary from 0.01 to  $1 \times 10^{-18}$  m<sup>2</sup> /BRA 80/. Laboratory values and those from regional studies in argillaceous media at porosities between 0.1 and 0.4 were reported to vary in the range  $10^{-23}$ – $10^{-17}$  m<sup>2</sup> /NEU 94/. Permeabilities measured for unreacted and reacted bentonites here are within this range as well (Tab. 3.5, Fig. 3.14, Fig. 3.15). Unreacted B04 and SD80 from Milos (Greece) at dry densities of 1.52–1.53 g/cm<sup>3</sup> show the lowest average permeability of about  $6.9 \times 10^{-20}$  m<sup>2</sup>, which is comparable to a permeability of  $9.2 - 9.4 \times 10^{-20}$  m<sup>2</sup> (calculated from the reported hydraulic conductivities) measured for a 2 M NaCl solution and GMZ01 bentonite at a higher dry density of 1.70 g/cm<sup>3</sup> /ZHU 13/, /CHE 15/. According to /JOB 17b/ the integral permeability of bentonite-based barriers in repository concepts in German clay formations should not exceed  $2 \times 10^{-17}$  m<sup>2</sup>.

**Tab. 3.5** Swelling pressures  $P_{s,u}$  of unreacted bentonites and  $P_{s,r}$  of bentonites reacted with VGH for  $430 \pm 11$  days at  $25^\circ\text{C}$  before and after fluid pressure surges of 12.6 MPa in the first<sup>§</sup> and 0.3 MPa in the second<sup>&</sup> series of permeameter experiments. Permeabilities  $p_u$  of unreacted and  $p_r$  of reacted bentonites are given as measured after the surges<sup>%</sup>

	$P_{s,u}$ , MPa (before surge)	$P_{s,u}$ , MPa (after surge)	$p_u$ , m <sup>2</sup>	$P_{s,r}$ , MPa & (before surge)	$P_{s,r}$ , MPa & (after surge)	$p_r$ , m <sup>2</sup>
B04	$3.64 \pm 0.01$	$2.48 \pm 0.01$	$8.1 \times 10^{-20}$	$1.40 \pm 0.01$	$0.48 \pm 0.01$	$1.9 \times 10^{-18}$
B09	$1.26 \pm 0.01$	$0.75 \pm 0.01$	$1.1 \times 10^{-18}$	$0.13 \pm 0.04^*$	$0.21 \pm 0.05^*$	$5.4 \times 10^{-18}$
B10	$3.91 \pm 0.01^{\&}$	$3.91 \pm 0.01^{\&}$	— <sup>#</sup>	$0.54 \pm 0.05^*$	$0.20 \pm 0.03^*$	$1.7 \times 10^{-18}$
B11	$2.30 \pm 0.01$	$1.99 \pm 0.01$	$3.9 \times 10^{-19}$	$0.30 \pm 0.04^*$	$0.19 \pm 0.09^*$	$5.4 \times 10^{-18}$
B12	$0.35 \pm 0.01$	$0.17 \pm 0.01$	$2.0 \times 10^{-18}$	$1.09 \pm 0.05^*$	$0.68 \pm 0.09^*$	$9.9 \times 10^{-19}$
B13	$2.89 \pm 0.01$	$1.99 \pm 0.01$	$6.1 \times 10^{-19}$	$1.02 \pm 0.01$	$0.72 \pm 0.01$	$2.7 \times 10^{-18}$
B16	$1.18 \pm 0.01$	$0.93 \pm 0.01$	$2.1 \times 10^{-18}$	$0.19 \pm 0.05^*$	$0.37 \pm 0.08^*$	$5.2 \times 10^{-18}$
B19	$0.73 \pm 0.01$ $0.88 \pm 0.02^{\&}$	$0.53 \pm 0.01$ $0.86 \pm 0.02^{\&}$	$3.1 \times 10^{-18}$ $1.6 \times 10^{-18}$	$0.93 \pm 0.01$	$0.72 \pm 0.01$	$4.3 \times 10^{-18}$
B23	$0.00 \pm 0.01$	$0.00 \pm 0.02$	$3.0 \times 10^{-17}$	$0.48 \pm 0.05^*$	$0.51 \pm 0.09^*$	$2.3 \times 10^{-18}$
B31	$4.72 \pm 0.01$	$3.94 \pm 0.01$	$5.0 \times 10^{-19}$	$0.78 \pm 0.02$	$0.52 \pm 0.02$	$2.6 \times 10^{-18}$
B36	$2.67 \pm 0.01$	$2.13 \pm 0.01$	$9.7 \times 10^{-18}$	$0.69 \pm 0.07^*$ $0.69 \pm 0.01$	$0.91 \pm 0.09^*$	$1.0 \times 10^{-17}$ $1.4 \times 10^{-17}$
B37	$0.31 \pm 0.01$	$0.31 \pm 0.01$	$2.0 \times 10^{-17}$	$1.39 \pm 0.04$	$0.89 \pm 0.01$	$4.1 \times 10^{-19}$
B38	$1.60 \pm 0.01^{\&}$	$1.63 \pm 0.01^{\&}$	$1.9 \times 10^{-18}$	$0.55 \pm 0.01$	$0.56 \pm 0.01$	$1.8 \times 10^{-17}$
B49	$4.28 \pm 0.06^{\&}$	$3.25 \pm 0.01^{\&}$	$1.0 \times 10^{-18}$	$1.98 \pm 0.05^*$	$1.73 \pm 0.08^*$	$2.4 \times 10^{-18}$
SD80	$4.85 \pm 0.01^{\&}$	$4.98 \pm 0.02^{\&}$	$6.9 \times 10^{-20}$	$1.34 \pm 0.01$ $2.21 \pm 0.01$	$1.28 \pm 0.01$	$6.9 \times 10^{-19}$ $2.5 \times 10^{-19}$

\* values obtained with force transducers from burster (see discussion to Fig. 2.8)

% results of replicate measurements for B19, B36, and SD80 are given as well

# no value could be obtained because of absent percolation through bentonite pellet

It can be seen from the present data that at the applied dry densities in the range 1.47–1.59 g/cm<sup>3</sup> all unreacted bentonites except for B23 and all reacted bentonites would comply with this requirement, albeit the average permeabilities of  $1.8 \times 10^{-17}$  m<sup>2</sup> for unreacted B37 and reacted B38 lie very close to this limit. A comparison for unreacted and reacted bentonites shows further that only for B12, B23, and B37, a significant increase of swelling pressure (after surge) and a decrease of permeability occurred upon the reaction (Tab. 3.5). Establishing reasons for this deviating behaviour would require microstructural analyses and was beyond the scope of the present study.

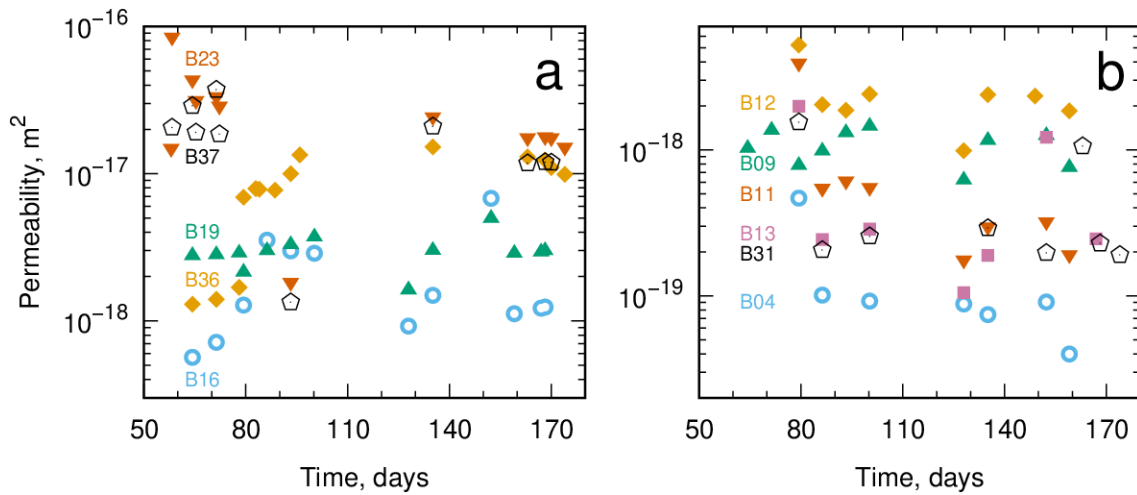


**Fig. 3.14** Evolution of permeability for VGH ( $\text{m}^2$ ) of unreacted bentonites in the first series

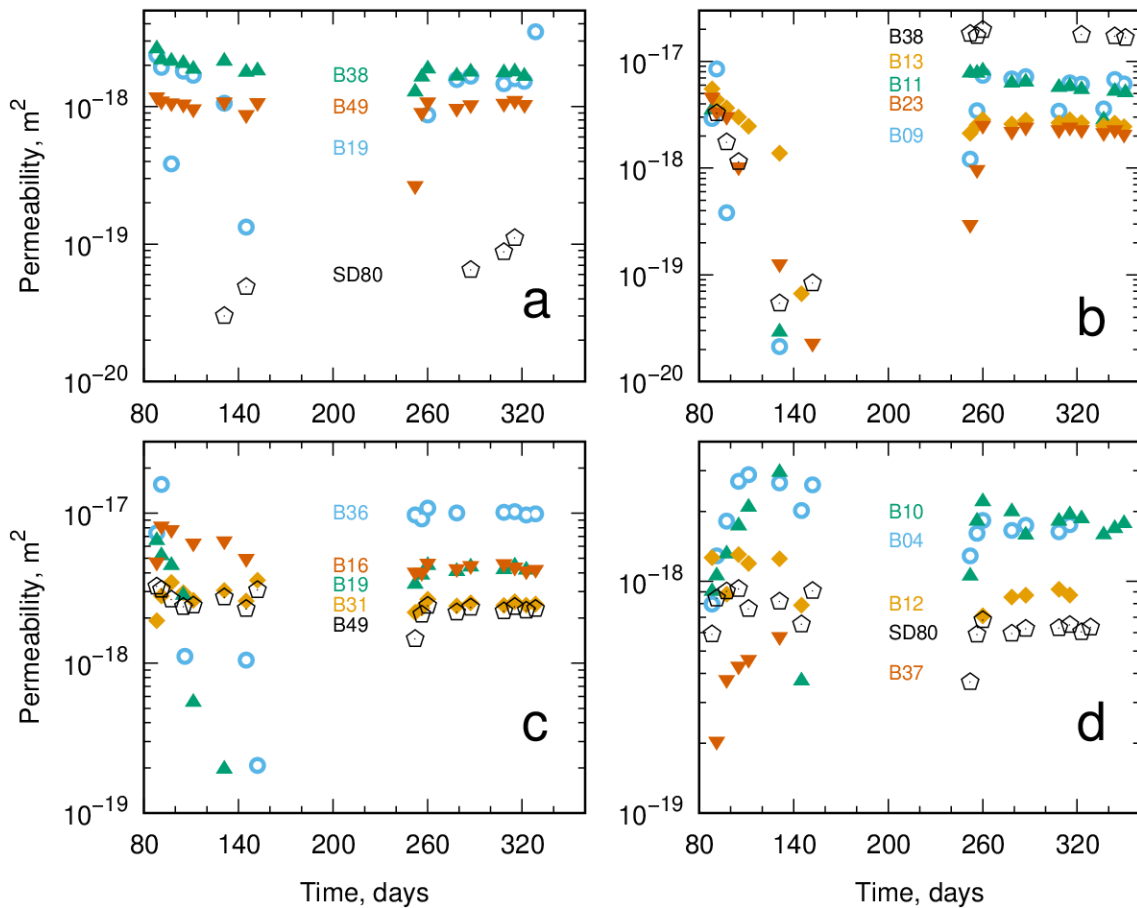


**Fig. 3.15** Evolution of permeability for VGH ( $\text{m}^2$ ) of unreacted bentonites (a) and bentonites reacted with VGH for  $430 \pm 11$  days at  $25 \text{ }^\circ\text{C}$  (b–d) in the second series

### 3.3.2 Effect of microstructural re-organization

Bentonite swelling behaviour observed in many studies upon saturation with solutions of low salinity (as discussed, e.g., by /YIG 16/) is characterized by a rapid initial increase (e.g., within 10 hours for GMZ01 bentonite in /ZHU 13/), followed by an intermediate period where the swelling pressure decreases, and a second increase (e.g., after about 30–40 hours for GMZ01 bentonite in /YE 13/, /ZHU 13/) to a final steady-state value. This “double-peak” pattern of swelling pressure evolution is explained by (i) a rapid swelling of aggregates (the first peak), followed by (ii) a deformation and, upon a sufficient hydration, a partial decomposition of aggregates with an accompanying collapse of the pores between the aggregates (depression after the first peak), and (iii) the final swelling of the then re-organized and partially smaller aggregates (the second peak) /YIG 16/. At dissolved salt concentrations above ~0.5 M, only the first peak was observed for GMZ01 bentonite in /ZHU 13/.

Although VGH is characterized by a considerably higher dissolved salt concentration of 2.6 M, the double-peak pattern of swelling pressure evolution was still observed for unreacted B04, B13, B16, and B31 (Fig. 3.16). This observation suggests that the occurrence of the double-peak pattern at higher salinities of saturating solutions may depend on bentonite identity. Swelling pressure evolution observed here features a higher second peak for unreacted bentonites B04 and B13, similarly to the observations by /YE 13/, /ZHU 13/, /YIG 16/ and references therein, but, differently from those works, a lower second peak for unreacted bentonites B16 and B31. A reason for this observation might be the high salinity of saturating VGH.

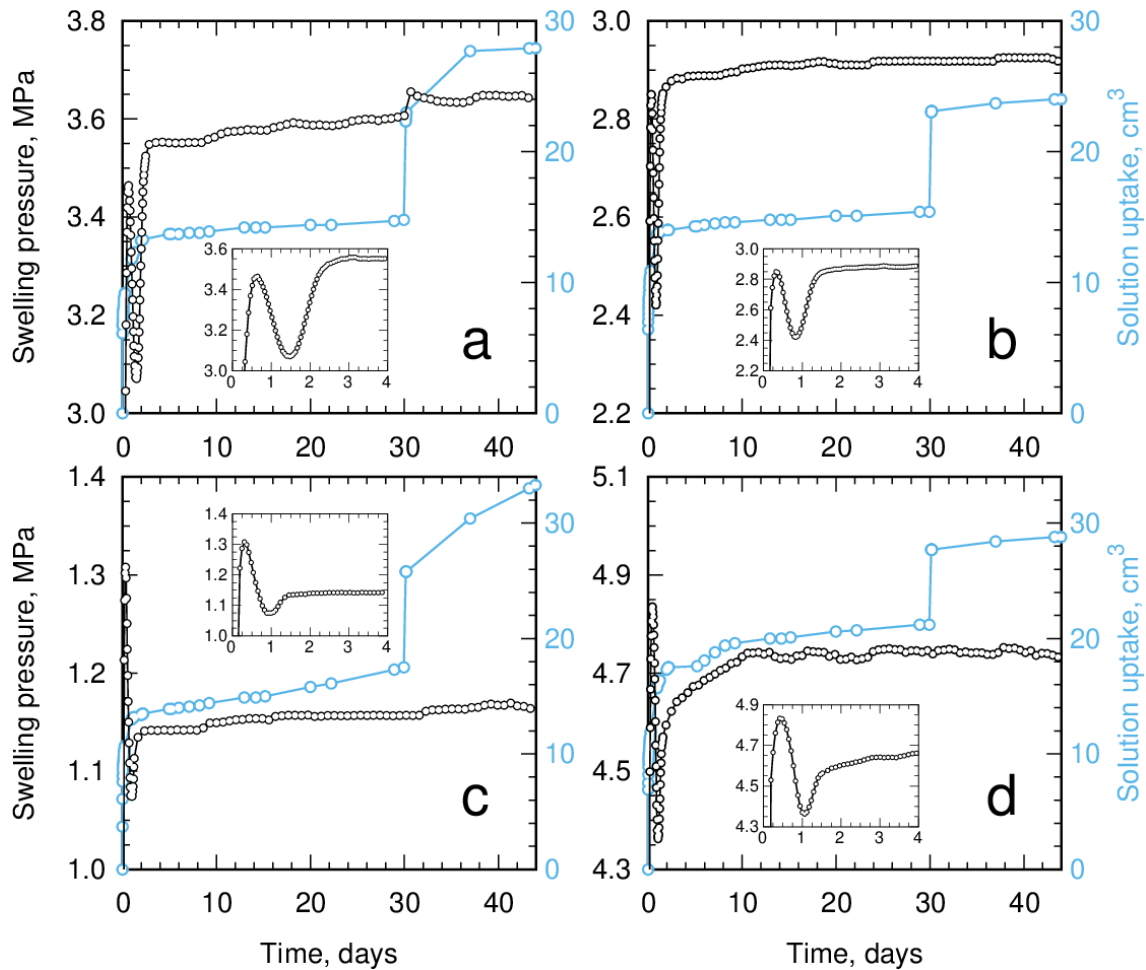


**Fig. 3.16** Swelling pressure and solution uptake for unreacted B04 (a), B13 (b), B16 (c), and B31 (d) at respective dry densities of 1.52, 1.52, 1.54, and 1.57 g/cm<sup>3</sup> upon saturation with VGH (supplied by burettes connected to inlets at cell bottoms for 30 days and at cell tops afterwards). Insets show close-ups for the first four days of saturation

It can be further seen from Fig. 3.16 that although compacted bentonite absorbed 8 up to 16 ml solution from burettes connected to inlets at cell tops after 30 days, which made 50 up to nearly 100 % of the water amount absorbed previously through the inlets at cell bottoms, no according increase of swelling pressure occurred, except for a small one for B04. This may suggest that the interlayer nanopores and intra-aggregate micropores, responsible for the swelling pressure evolution as discussed before, at the top side of bentonite pellets were already saturated with water, except, probably, for a small portion of such pores in B04. Accordingly, the solution arriving from the cell tops would only saturate the inter-aggregate macropores hardly contributing to the macroscopic swelling pressure.

It is noticeable that differently from the swelling behaviour in the first series, characterised by a rapid initial increase of swelling pressure (Fig. 3.16, Fig. 3.17), no such increase and, correspondingly, no double-peak pattern were observed in the second series for both, unreacted and reacted bentonites (Fig. 3.18). A probable reason for this observation may be the triple loading/unloading of compacted bentonites in advance of the contact with VGH applied in the second series. Comparison of swelling behaviours observed for unreacted B19 in the first and the second series (Fig. 3.17a, Fig. 3.18b) support this suggestion, as the triple loading/unloading was the only major difference in the preparation of the two tests with this bentonite.

A preliminary desiccation of bentonites at high suction pressures was found to cause a destruction of large aggregates and microstructural reorganization accompanied by an increase swelling pressure /LAN 18/ in a process apparently very similar or identical to that occurring during hydration as discussed at the beginning of this section. An assumption that the energy supplied during the loading/unloading suffice for triggering a destruction of large aggregates and microstructural reorganization might then explain the lacking double-peak pattern of swelling pressure evolution and the lacking rapid increase of swelling pressure in the second series. The observed decreases of stress necessary to compact bentonites B10, B38, and SD80 to the prescribed density of 1.6 g/cm<sup>3</sup> during the consecutive loadings (Fig. 3.19) indicate microstructure adjustments during the preceding unloadings which may support this argumentation.

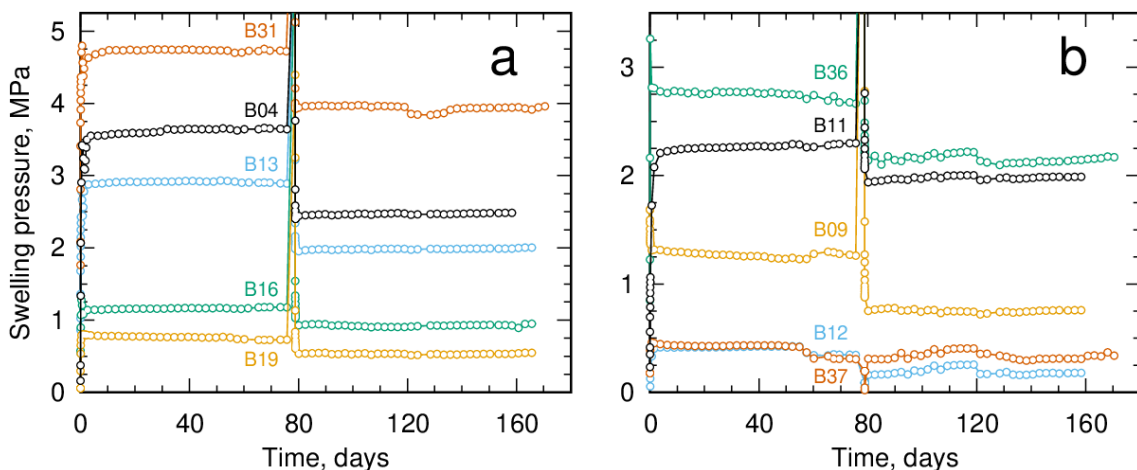


**Fig. 3.17** Swelling pressure evolution for unreacted (a) B04, B13, B16, B19, and B31, and (b) B09, B11, B12, B36, and B37 at dry densities in the range 1.51–1.59 g/cm<sup>3</sup> upon saturation with VGH in the first series. VGH was supplied by burettes for 44 to 57 days and by a pump afterwards

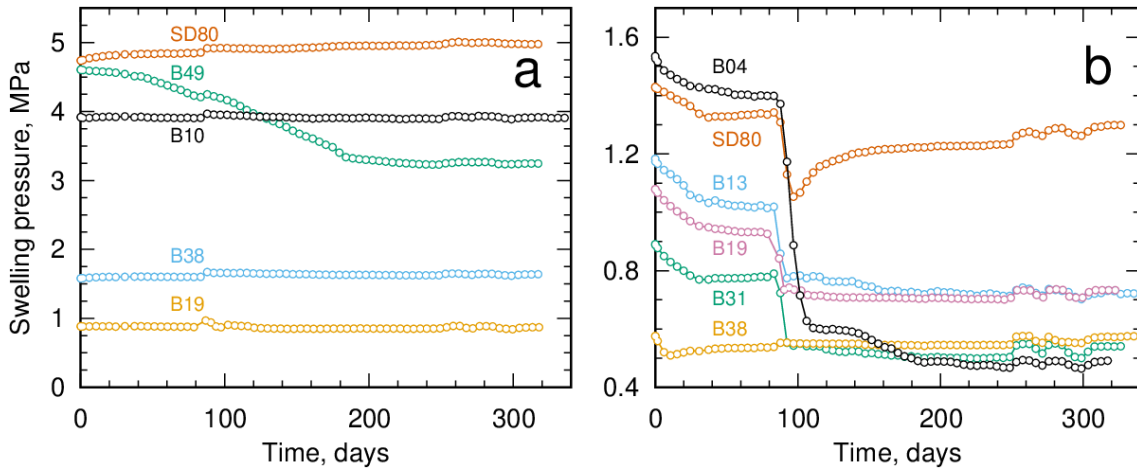


**Fig. 3.18** Swelling pressure evolution for (a) unreacted B10, B19, B38, B49, and SD80 at dry densities in the range 1.47–1.55 g/cm<sup>3</sup>, and (b) B04, B13, B19, B31, B38, and SD80 after reaction with VGH for 430 ± 11 days at 25°C upon saturation with VGH in the second series. VGH was supplied by burettes for 75 days and by a pump afterwards

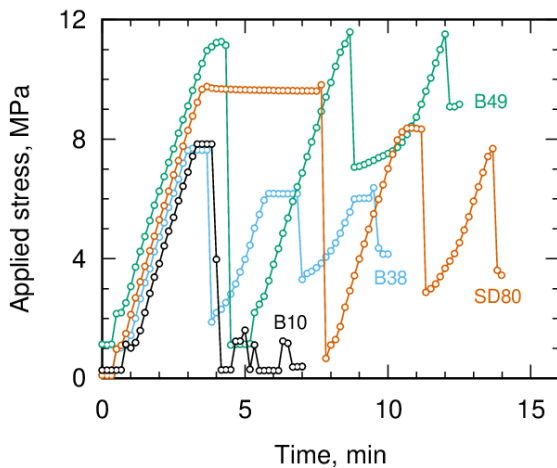


**Fig. 3.19** Stress applied to compact B10, B38, B49, and SD80 to a density of 1.6 g/cm<sup>3</sup> in the first loading followed by an unloading and two further loadings/unloadings

Yet, such stress decreases do not occur for B49 (Fig. 3.19), which might be putatively attributed to some reorganisational reluctance pertinent to its microstructure. Indeed, differently from the other unreacted bentonites, B49 did not show a rapid microstructure reorganization upon saturation with VGH but rather a very slow one over a period of about 180 days (Fig. 3.18a).

### 3.3.3 Effect of fluid pressure surges

In the first series, pressure of solution supplied to the bottoms of permeameter cells surged from 0.2 to 12.6 MPa on the 78<sup>th</sup> day and remained at this level for about 45 min (Fig. 2.9), which caused considerable decreases of swelling pressure by 13 up to 51% for 9 of 11 bentonites at the end of this time interval (Fig. 3.17, Tab. 3.5). Upon this fluid pressure surge, force transducers in the cell tops registered an additional load of 6.1 MPa for B19, 9.8–10.2 MPa for B04, B11, B13, and B16, 10.9 MPa for B09, 11.7 MPa for B36, and 12.2 MPa for B31 (no records during the pressure surge were delivered by force transducers in tests with B12 and B37 presumably because of overload).

The fact that the fluid pressure of 12.6 MPa remained nearly unchanged during the whole duration of pressure surge (~45 min), after which the pump restored the prescribed fluid injection pressure of 0.2 MPa (Fig. 2.9), evidences that no hydraulic fracture formed in the bentonite pellets. The accompanying additional loads recorded by force transducers can be then inferred to result from the increased mechanical stress on the pellets, which was passed down to the force transducers by the mineral skeleton of pellets. The different mechanical loads passed down to the force transducers by different bentonites can be accordingly explained by different extent of microstructural deformations in bentonites.

Furthermore, no considerable increase of volume of solution infiltrating through pellets, which would also evidence hydraulic fracturing inside pellets or at their interface with cell walls, occurred for studied bentonites (Fig. 3.14a). Although permeability increased for B16 and B36 by a factor of 1.8 and 4.1, respectively, upon the pressure surge, it remained at a low level of  $1.3\text{--}6.9 \times 10^{-18} \text{ m}^2$ , which evidences that no fracture flow occurred through these bentonites. The first solution percolation through bentonites B04, B11–B13, and B31 occurred on the next day after the pressure surge (Fig. 3.14b), which indicates a cause-effect relationship between these events. However, their permeabilities calculated assuming that percolation started upon the pressure surge were in the range  $4.7 \times 10^{-19}\text{--}5.2 \times 10^{-18} \text{ m}^2$  (Fig. 3.14b), which evidences that no advective flow occurred through these bentonites either. Eight days later, of these bentonites decreased down to  $1.0 \times 10^{-19}$  to  $2.0 \times 10^{-18} \text{ m}^2$  (Fig. 3.14b).

In experiments with bentonite Kunigel V1 compacted to a dry density of  $1.6 \text{ g/cm}^3$ , the onset of hydraulic fracturing was observed within several minutes upon increasing the fluid injection pressure to threshold values of 3.2 up to 4.7 MPa, whereas for its 70:30 mixture with sand even broader variation of threshold values from 2 to

8 MPa was measured /KOB 08/. The question than arises, why bentonites studied here are characterized by a much higher strength for hydraulic fracturing of at least 12.6 MPa than Kunigel V1. Swelling pressure, which was argued to strongly influence the breakdown pressure /KOB 08/, varies broadly for studied bentonites (Tab. 3.5) below and above the value of 1.8 MPa measured for Kunigel V1 /KOB 08/ and, hence, cannot be a reason for this difference. Similarly, the water content, increase of which was argued to decrease the strength for hydraulic fracturing /KOB 08/, cannot be a reason for this difference as well, as at the time of pressure surge studied bentonites were saturated with water and its content (around 25 %) was much higher than that of 12.5 % for Kunigel V1 /KOB 08/. It ought to be then concluded that the reason for the difference can be the different experimental setup used in /KOB 08/, which featured a tube with a diameter of 2 mm for a point-wise injection of water into an unsaturated bentonite compacted around the tube. Such a setup appears to be not transferable to the setup in the present study with the solution being injected over a surface with an area of 19.6 cm<sup>2</sup> from outside the compacted bentonite, which is thought to closer resemble the expected situation in a repository.

In the second series, the fluid pressure surged upon the switching on the pump from 0 to 0.28 MPa and then to 0.44 MPa with the consequence that swelling pressures decreased within about two (B13) to 20 (B04) days in a first, relatively steep step and within further up to 80 days (B04) in a second, more gradual step by up to 66 % for 9 of 15 reacted bentonites (Fig. 3.18b, Tab. 3.5). Tests with B19 (Fig. 3.18) illustrate that one-year reaction with VGH at 25 °C can apparently cause some relevant changes of its microstructure, as its swelling pressure decreased by 23 % while that of unreacted B19 did not show any significant change upon the same fluid pressure surge. A mode of microstructural modification obviously deviating from that for the other studied bentonites was observed for reacted SD80, swelling pressure of which decreased by 0.37 MPa within 10 days after the fluid pressure surge, but increased steadily afterwards and nearly reached the original value at the end of the test (Fig. 3.18b).

Presented data allow to suggest that the decreases of swelling pressure upon fluid pressure surges must originate from a process leading depending on bentonite type to different modes of microstructural reorganisation. An additional compaction of bentonite pellets during the pressure surge, which would lead to a decreased pellet height and to an accordingly decreased force exerted by pellet on the force transducers of the permeameter cell, can be discarded as a possible reason

considering that in the second series this process proceeds rather slowly, on the scale of several days to several weeks (Fig. 3.18b). This process may be a reverse one to that of destruction of large aggregates discussed in the preceding section and lead to a formation of larger aggregates and larger pores in bentonite and thus to lower macroscopic swelling pressures.



## 4 Concluding remarks

Until now, it was assumed in safety assessments of geological repositories of high-level radioactive waste that calcite and other carbonate minerals become more stable and precipitate at elevated temperatures, as discussed, e.g., in /WER 07/, /BRA 14/. The present study shows that this assumption is not valid for carbonate minerals in bentonites presumably because of the carbonate–clay interaction. Carbonate dissolution and a loss of up to 1.7 and 2.1 % of bentonite mass per year at 90 °C and 120 °C, respectively, and a loss of at least of 0.2 % of bentonite mass per year at 25 °C were observed. Furthermore, CO<sub>2</sub> releases and CO<sub>2</sub> partial pressures of up to 2 bar upon a contact of bentonites with both, a brine (VGH) and a highly saline water (OPA) at 90 °C and 120 °C were shown to occur at the studied experimental conditions.

From these observations, several open questions were identified which need to be answered in order to understand the observed untrivial dependence of carbonate dissolution and CO<sub>2</sub> release on bentonite identity, solution composition, and bentonite-solution mass ratio. Most importantly, it remains to be determined which non-carbonate mineral components of bentonite and in which way influence carbonate dissolution and CO<sub>2</sub> release and whether a possible different reactivity of carbonate minerals in different bentonites may modify the characteristics of this process.

As discussed above, a cancellation of the buffering capacity of bentonites because of a sufficiently high increase of CO<sub>2</sub> partial pressure may lead to a decrease of pH to acidic values and, consequently, to increased corrosion rates of metallic components of a repository. An increase of gas pressure due to CO<sub>2</sub> release and a modification of mechanical properties due to loss of constituting carbonate minerals in clay-based barriers in the near field of a geological repository represent two other potentially important safety issues related to carbonate dissolution. This exemplifies the need for a thorough understanding of the mechanism of CO<sub>2</sub> release in clays.

The results of pH measurements suggest that reaction times of at least one to two years may be necessary for a realistic estimation of equilibrium pH values of bentonite suspensions. A mere contact of bentonite with brine at 25°C but also a prolonged heating of bentonite-brine suspension at 90°C or 120°C may strongly deteriorate its buffering capacities as manifested by the observed acidic pH. The mineralogical reasons for this acidification effect of brine and of high temperatures need to be addressed in a follow-

up study in order to be able to properly consider possible pH decreases to acidic values in clay-based barriers in long-term repository assessments.

No hydraulic fracturing occurred in compacted unreacted bentonites as a result of the fluid pressure surge of 12.6 MPa. This observation challenges the validity of threshold values of a few MPa for onset of hydraulic fracturing in compacted bentonites proposed earlier using an alternative experimental method /KOB 08/. However this pressure surge led to a twofold decrease of their swelling pressures, presumably, as a result of a plastic deformation in compacted bentonites, which partially absorbed the energy input of the pressure surge. Similar decreases of swelling pressures occurred for bentonites compacted after their one-year reaction with VGH at 25°C upon a much smaller fluid pressure increase of 0.3 MPa. It remains to be understood which microstructural changes are responsible for these macroscopic observations. Provided independent confirmation of the reported observations and that occurrence of fluid pressure surges either as a result of gas accumulation and release or other processes in repository can represent a possible scenario of its evolution, gaining such understanding would be of particular importance for design of bentonite-based barriers and their performance assessments. It may be also reasonable to prove whether the effect of fluid pressure surges on compacted bentonites can be considered as a conservative limit for the effect of the expected gradual increase of fluid pressure in the course of restoration of hydraulic conditions in the host formation upon the repository closure.

Changes in swelling pressures and permeabilities of bentonites upon one-year reaction with VGH at 25 °C observed in the present study are summarized in Fig. 4.1 and Fig. 4.2.

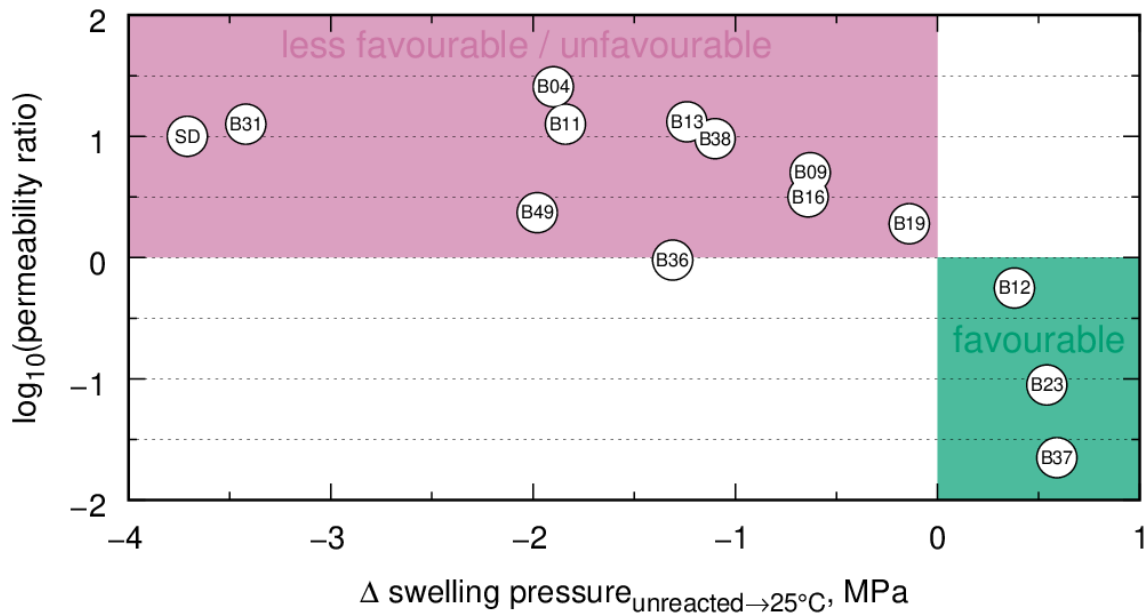


**Fig. 4.1** Changes of swelling pressures and permeabilities for bentonites upon a reaction with VGH for  $430 \pm 11$  days at  $25^\circ\text{C}$

Fig. 4.1 illustrates that as discussed above, B23 and B37 show the most favourable – with respect to the isolating properties of bentonite-based barrier – changes of swelling pressure and permeability upon reaction with VGH, whereas SD80 and B31 show the most unfavourable changes of swelling pressure and B04 that of permeability. However, the data on residual values of swelling pressure and permeability in Fig. 4.2 reveals a more differentiated picture. Despite the strong decrease, the swelling pressure of reacted SD80 remains the second highest one (top panel in Fig. 4.2) and its permeability remains the second lowest one (bottom panel in Fig. 4.2). Reacted B04 appears to show just a mid-level permeability, whereas B38 shows the highest permeability. Whereas reacted B37 shows the lowest permeability and the third highest swelling pressure, B23 shows only mid-level values. Furthermore, B12 and B19 appear to be the most stable with respect to interaction with VGH at  $25^\circ\text{C}$ .

The key question is then whether the changes observed here after one-year reaction with VGH would proceed with similar intensity, so that, e.g., the swelling pressure of SD80 would be lower than that of B37 after a certain time, or bentonites have adjusted to VGH and no unfavourable changes would occur, so that, e.g., SD80 would be a better candidate than B37 for the use as barrier material based on swelling pressure and permeability values. This question could not be answered in the present study and should be approached in a follow-up study.

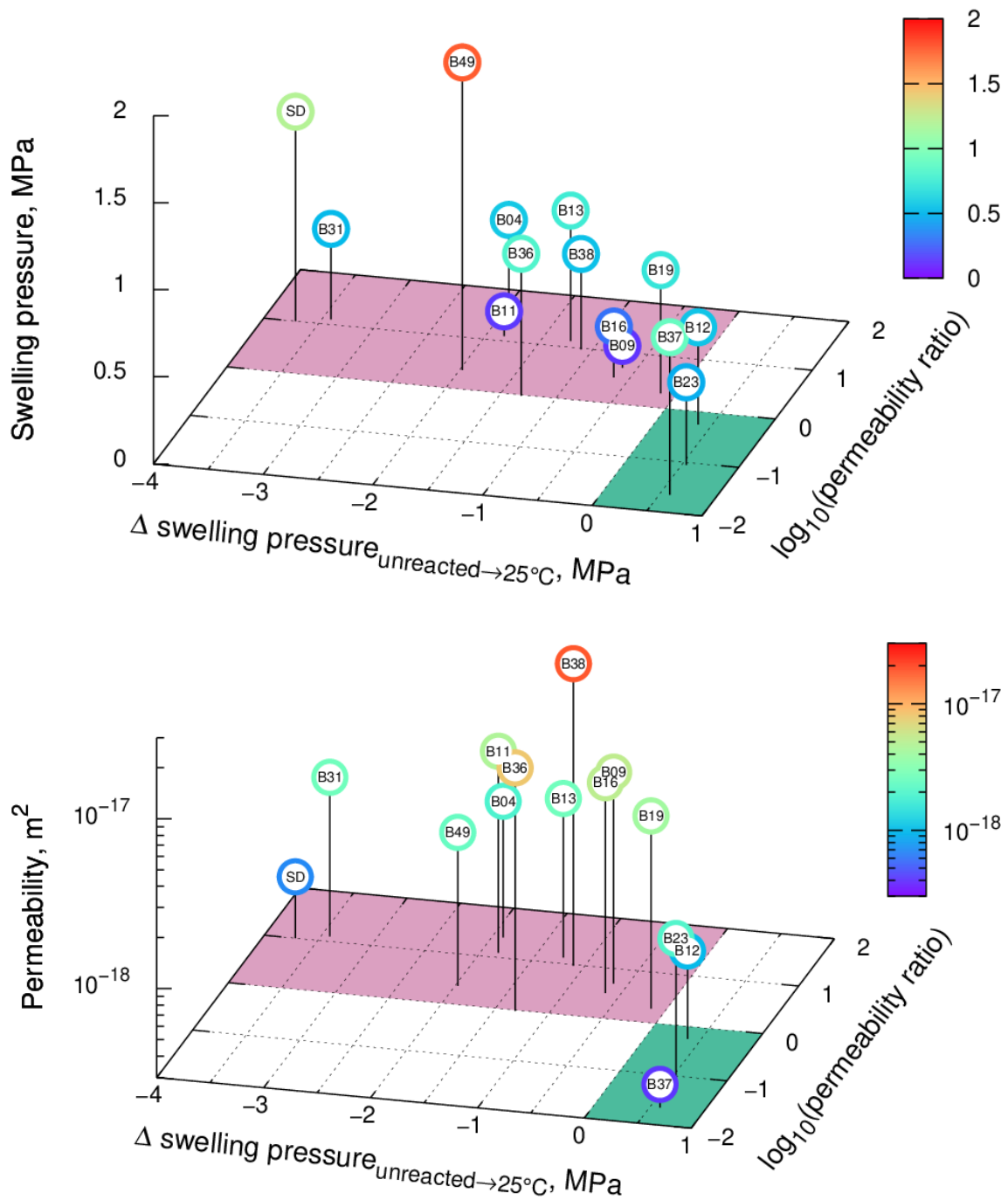


**Fig. 4.2** Swelling pressures (top panel) and permeabilities (bottom panel) of bentonites reacted with VGH for  $430 \pm 11$  days at 25°C upon their changes with respect to those of unreacted bentonites

Considering the preceding discussion and discussion on pH changes, an in-depth study involving B16 (strongest pH decrease, stable swelling pressure and permeability), B19 (stable pH, swelling pressure and permeability), B37 (strong pH decrease, strongest swelling pressure and permeability increases), and SD80 (stable pH, strongest swelling pressure and strong permeability decreases) can be suggested.



## Literature

- /AMO 98/ Amonette, J. E., & Templeton, J. C. (1998). Improvements to the quantitative assay of nonrefractory minerals for Fe (II) and total Fe using 1, 10-phenanthroline. *Clays and Clay Minerals* 46, 51-62.
- /ANA 08/ Anastácio, A. S., Harris, B., Yoo, H., Fabris, J. D., & Stucki, J. W. (2008). Limitations of the ferrozine method for quantitative assay of mineral systems for ferrous and total iron. *Geochemica et Cosmochimica Acta* 72, 5001–5008.
- /BIR 81/ Birch, G. F. (1981). The Karbonat-Bombe: a precise, rapid and cheap instrument for determining calcium carbonate in sediments and rocks. *Transactions of the Geological Society of South Africa* 84, 199-203.
- /BRA 80/ Brace, W. F. (1980). Permeability of crystalline and argillaceous rocks. *International Journal of Rock Mechanics and Mining Sciences & Geomechanics Abstracts* 17, 241-251.
- /BRA 02/ Bradbury, M. H., & Baeyens, B. (2002). Porewater chemistry in compacted re-saturated MX-80 bentonite: Physico-chemical characterisation and geochemical modelling. Technical Report 01-08, Nagra, Switzerland.
- /BRA 14/ Bradbury, M. H., Berner, U., Curti, E., Hummel, W., Kosakowski, G., & Thoenen, T. (2014). The long term geochemical evolution of the near-field of the HLW repository. Technical Report 12-01, Nagra, Switzerland.
- /BRU 12/ Bruggeman, C., & Craen, M. de (2012). Boom Clay natural organic matter. Report ER-206, SCK-CEN, Belgium.
- /CER 17/ Ceriotti, G., Porta, G. M., Geloni, C., Dalla Rosa, M., & Guadagnini, A. (2017). Quantification of CO<sub>2</sub> generation in sedimentary basins through carbonate/clays reactions with uncertain thermodynamic parameters. *Geochimica et Cosmochimica Acta* 213, 198-215.
- /CHE 15/ Chen, Y. G., Zhu, C. M., Ye, W. M., Cui, Y. J., & Wang, Q. (2015). Swelling pressure and hydraulic conductivity of compacted GMZ01 bentonite under salinization–desalinization cycle conditions. *Applied Clay Science* 114, 454-460.

- /CHE 16/ Chen, Y. G., Jia, L. Y., Ye, W. M., Chen, B., & Cui, Y. J. (2016). Advances in experimental investigation on hydraulic fracturing behavior of bentonite-based materials used for HLW disposal. *Environmental Earth Sciences* 75, 1-14.
- /COU 98/ Coudrain-Ribstein, A., Gouze, P., & Marsily, G. de (1998). Temperature-carbon dioxide partial pressure trends in confined aquifers. *Chemical Geology* 145, 73-89.
- /FAB 68/ Fabuss, B. M., & Korosi, A. (1968). Properties of sea water and solutions containing sodium chloride, potassium chloride, sodium sulfate and magnesium sulfate. U.S. Department of the Interior, Office of Saline Water, Washington D.C.
- /FIL 17/ Filipská, P., Zeman, J., Všianský, D., Honť, M., & Škoda, R. (2017). Key processes of long-term bentonite-water interaction at 90 °C, Mineralogical and chemical transformations. *Applied Clay Science* 150, 234-243.
- /HOM 03/ Homm, K., & Wehner, H. (2003). Organische Geochemie, Organische Petrographie und thermische Versuche an Tonsteinen aus der Bohrung Uthmöden 1/60. Report, BGR, Hannover, 91 p.
- /HUT 90a/ Hutcheon, I., Abercrombie, H. J., & Krouse, H.R. (1990). Inorganic origin of carbon dioxide during low temperature thermal recovery of bitumen. Chemical and isotopic evidence. *Geochimica et Cosmochimica Acta* 54, 165–171.
- /HUT 90b/ Hutcheon, I., & Abercrombie, H. (1990). Carbon dioxide in clastic rocks and silicate hydrolysis. *Geology* 18, 541–544.
- /JOB 17a/ Jobmann, M., Bebiolka, A., Burlaka, V., Herold, P., Jahn, S., Lommerzheim, A., Maßmann, J., Meleshyn, A., Mrugalla, S., Reinhold, K., Rübél, A., Stark, L., & Ziefle, G. (2017). Safety assessment methodology for a German high-level waste repository in clay formations. *Journal of Rock Mechanics and Geotechnical Engineering* 9, 856–876.
- /JOB 17b/ Jobmann, M., Bebiolka, A., Jahn, S., Lommerzheim, A., Maßmann, J., Meleshyn, A., Mrugalla, S., Reinhold, K., Rübél, A., Stark, L. & Ziefle, G. (2017). Sicherheits- und Nachweismethodik für ein Endlager im Tongestein in Deutschland – Synthesebericht. Ber.-Nr.: TEC-13-2016-AB, DBE TECHNOLOGY GmbH, BGR, GRS; Peine, Hannover, Braunschweig.

- /JOC 08/ Jockwer, N., & Wieczorek, K. (2008). Investigations on gas generation, release, and migration in the frame of FEBEX. Report GRS-243, GRS, Braunschweig.
- /KAR 06/ Karnland, O., Olsson, S., & Nilsson, U. (2006). Mineralogy and sealing properties of various bentonites and smectite-rich clay materials. Report TR-06-30, SKB, Stockholm.
- /KAU 08/ Kaufhold, S., & Dohrmann, R. (2008). Detachment of colloidal particles from bentonites in water. *Applied Clay Science* 39, 50-59.
- /KAU 12/ Kaufhold, S., Hein, M., Dohrmann, R., & Ufer, K. (2012). Quantification of the mineralogical composition of clays using FTIR spectroscopy. *Vibrational Spectroscopy* 59, 29-39.
- /KAU 13/ Kaufhold, S., Plötze, M., Klinkenberg, M., & Dohrmann, R. (2013). Density and porosity of bentonites. *Journal of Porous Materials* 20, 191-208.
- /KLO 94/ Klosa, D. (1994). Eine rechnergestützte Methode zur Bestimmung des Gesamtkarbonatgehaltes in Sedimenten und Böden. *Z. angew. Geol.* 40, 18–21.
- /KOB 08/ Kobayashi, A., Yamamoto, K., & Momoki, S. (2008). Characteristics of strength for hydraulic fracturing of buffer material. *Soils and Foundations* 48, 467–477.
- /LAN 18/ Lang, L. Z., Baille, W., Tripathy, S., & Schanz, T. (2018). Experimental study on the influence of preliminary desiccation on the swelling pressure and hydraulic conductivity of compacted bentonite. *Clay Minerals* 53, 733–744.
- /LIU 11/ Liu, D., Dong, H., Bishop, M. E., Wang, H., Agrawal, A., Tritschler, S., Eberl, D. D., & Xie, S. (2011). Reduction of structural Fe(III) in nontronite by methanogen *Methanosarcina barkeri*. *Geochimica et Cosmochimica Acta* 75, 1057–1071.
- /LLO 07/ Lloret, A., & Villar, M. V. (2007). Advances on the knowledge of the thermo-hydro-mechanical behaviour of heavily compacted “FEBEX” bentonite. *Physics and Chemistry of the Earth, Parts A/B/C* 32, 701–715.

- /LOR 08/ Lorant, F., Largeau, C., Behar, F., & Cannière, P. de (2008): Improved kinetic modeling of the early generation of CO<sub>2</sub> from the Boom Clay kerogen. Implications for simulation of CO<sub>2</sub> production upon disposal of high activity nuclear waste. *Organic Geochemistry* 39, 1294-1301.
- /MÜL 71/ Müller, G., & Gastner, M. (1971). The "Karbonat-Bombe", a simple device for the determination of carbonate content in sediment, soils, and other materials. *Neues Jahrbuch für Mineralogie-Monatshefte* 10, 466–469.
- /NEC 16/ Necib, S., Linard, Y., Crusset, D., Michau, N., Daumas, S., Burger, E., Romaine, A., & Schlegel, M. L. (2016). Corrosion at the carbon steel-clay borehole water and gas interfaces at 85 °C under anoxic and transient acidic conditions. *Corrosion Science* 111, 242–258.
- /NEU 94/ Neuzil, C. E. (1994). How permeable are clays and shales? *Water resources research* 30, 145–150.
- /PHI 81/ Phillips, S. L., Igbene, A., Fair, J. A., Ozbek, H., & Tavana, M. (1981). Technical databook for geothermal energy utilization (No. LBL-12810). Lawrence Berkeley Lab., CA (USA).
- /SCH 12/ Sherif, E. S. M., Almajid, A. A., Bairamov, A. K., & Al-Zahrani, E. (2012). A comparative study on the corrosion of monel-400 in aerated and de-aerated arabian gulf water and 3.5% sodium chloride solutions. *Int. J. Electrochem. Sci.* 7, 2796–2810.
- /SMI 89/ Smith, J. T., & Ehrenberg, S. N. (1989). Correlation of carbon dioxide abundance with temperature in clastic hydrocarbon reservoirs, Relationship to inorganic chemical equilibrium. *Marine and Petroleum Geology* 6, 129–135.
- /TRI 86/ Tributh, H., & Lagaly, G. (1986). Aufbereitung und Identifizierung von Boden- und Lagerstättentönen. I. Aufbereitung der Proben im Labor. *GIT-Fachzeitschrift für das Laboratorium* 30, 524–529.
- /WER 03/ Wersin, P. (2003). Geochemical modelling of bentonite porewater in high-level waste repositories. *Journal of Contaminant Hydrology* 61, 405–422.

- /WER 07/ Wersin, P., Johnson, L. H., McKinley, I. G. (2007). Performance of the bentonite barrier at temperatures beyond 100°C, A critical review. *Physics and Chemistry of the Earth* 32, 780–788.
- /YAU 87/ Yau, Y.-C., Peacor, D. R., Essene, E. J., Lee, J. H., Kuo, L.-C., & Cosca, M. A. (1987). Hydrothermal treatment of smectite, illite, and basalt to 460 degrees C; comparison of natural with hydrothermally formed clay minerals. *Clays and Clay Minerals* 35, 241–250.
- /YE 13/ Ye, W. M., Wan, M., Chen, B., Chen, Y. G., Cui, Y. J., & Wang, J. (2013). Temperature effects on the swelling pressure and saturated hydraulic conductivity of the compacted GMZ01 bentonite. *Environmental earth sciences* 68, 281–288.
- /YIG 16/ Yigzaw, Z. G., Cuisinier, O., Massat, L., & Masrouri, F. (2016). Role of different suction components on swelling behavior of compacted bentonites. *Applied Clay Science* 120, 81–90.
- /ZHU 13/ Zhu, C. M., Ye, W. M., Chen, Y. G., Chen, B., & Cui, Y. J. (2013). Influence of salt solutions on the swelling pressure and hydraulic conductivity of compacted GMZ01 bentonite. *Engineering Geology* 166, 74–80.



## List of Tables

<b>Tab. 2.1</b>	Chemical composition of VGH and OPA solutions .....	3
<b>Tab. 2.2</b>	Smectite content /KAU 12/ and exchangeable mono- and divalent cation contents /KAU 08/ of studied bentonites .....	4
<b>Tab. 3.1</b>	Carbonate contents (mass%) in unreacted bentonites (/KAU 12/, the present study) and in bentonites reacted with VGH for 374 days at 120 °C, and carbonate loss rate estimate (mass% per year) .....	15
<b>Tab. 3.2</b>	Vapour pressures (bar) for OPA and VGH at 90 °C and 120 °C and for diluted (200 g/l) and saturated (325 g/l) cap rock solutions at 120°C .....	18
<b>Tab. 3.3</b>	Headspace CO <sub>2</sub> and H <sub>2</sub> contents (ml) of bentonite and calcite suspensions with VGH and OPA after 91 and 146 days of reaction at 120 °C, respectively .....	21
<b>Tab. 3.4</b>	pH of VGH and OPA after reaction with B36 for one and two years at 25, 60, and 90 °C with (denoted by “μ”) and without substrate addition .....	28
<b>Tab. 3.5</b>	Swelling pressures $P_{s,u}$ of unreacted bentonites and $P_{s,r}$ of bentonites reacted with VGH for $430 \pm 11$ days at 25°C before and after fluid pressure surges of 12.6 MPa in the first <sup>§</sup> and 0.3 MPa in the second <sup>&amp;</sup> series of permeameter experiments. Permeabilities $p_u$ of unreacted and $p_r$ of reacted bentonites are given as measured after the surges% .....	33



## List of Figures

<b>Fig. 2.1</b>	Water contents (mass%) of unreacted bentonites calculated from the mass difference of the bentonite powder dried at 50°C for 3 up to 5 days and subsequently at 105°C for 3 up to 7 .....	5
<b>Fig. 2.2</b>	Left: disrupted and intact welded glass vessels in a drying oven after several hours of heating at 120 °C (inset: a welded glass vessel without aluminium foil). Right: alloy vessels with tubing to pressure transducers outside the oven and a gas sampling valve at the head piece (inset: gas sampling) .....	6
<b>Fig. 2.3</b>	A permeameter cell used in swelling pressure and permeability measurements (left), a construction drawing showing a vertical section of a permeameter cell (middle), and a hydraulic press used to compact bentonites within permeameter cells (right) .....	7
<b>Fig. 2.4</b>	Dry densities (g/cm <sup>3</sup> ) of unreacted compacted bentonites .....	8
<b>Fig. 2.5</b>	Burettes used to supply VGH to permeameter cells from cell bottoms (left) and cell tops (middle) and by a valve pump to measure the permeability (right, regard plastic vessels connected to cell tops to collect solutions percolating through bentonite pellets) .....	8
<b>Fig. 2.6</b>	Home-made carbonate bombs with attached pressure transducers connected to the data acquisition unit (left), a welded glass with 5 ml of 18 % HCl (middle) intended to disrupt upon an agitation after screwing on tight the carbonate bomb lid, and a magnetic stirrer (right) intended to stir the analysed powder material and the acid.....	9
<b>Fig. 2.7</b>	Average CO <sub>2</sub> pressures as a function of mass of dissolved CaCO <sub>3</sub> obtained from triple (double for 0.75 g CaCO <sub>3</sub> ) measurements. Coefficient of determination $R^2$ for linear regression of data (solid line: pressure = $(3.43 \pm 0.02) \times \text{mass} - (0.004 \pm 0.006)$ ) equals 1 .....	10

<b>Fig. 2.8</b>	Swelling pressure evolution (left, MPa) measured by force transducers from Ahlborn (middle, within the cap of the permeameter cell) for B38 and by those from burster (right) for B49.....	12
<b>Fig. 2.9</b>	A solution leak from the piston pump (left) and evolution of the fluid injection pressure (bar) during the first series (right). Inset shows a close-up of the fluid pressure surge .....	13
<b>Fig. 2.10</b>	Evolution of the fluid injection pressure (bar) during the second series (left) and salt encrustations within the syringe pump (right) .....	13
<b>Fig. 2.11</b>	Rust traces on the bottom side of unreacted B09 (left) and B23 (middle) pellets and on the porous steel plate in contact with B11 (right, no rust on B11 observed) after permeability measurements .....	14
<b>Fig. 3.1</b>	Gas pressure evolution for 1:2 suspensions of bentonites B10, B12, and B31 with VGH at 120 °C. Inset shows a close-up of the pressure evolution for B12 within the first day of reaction .....	17
<b>Fig. 3.2</b>	Gas pressure evolution of 1:2 bentonite suspensions with OPA at 120 °C. The initial mass of CaCO <sub>3</sub> in the batch vessel was calculated from the carbonate contents of unreacted bentonites (Tab. 3.1) .....	19
<b>Fig. 3.3</b>	Gas pressure evolution of 1:2 bentonite suspensions with VGH at 120 °C. The initial mass of CaCO <sub>3</sub> in the batch vessel was calculated from the carbonate contents of unreacted bentonites (Tab. 3.1) .....	19
<b>Fig. 3.4</b>	Gas pressure evolution of 1:2, 1:1, and 1:1/2 suspensions of bentonite B19 with OPA and VGH at 90 °C .....	22
<b>Fig. 3.5</b>	Gas pressure evolution of 1:2, 1:1, and 1:1/2 suspensions of bentonite B38 with OPA and VGH at 90 °C .....	22
<b>Fig. 3.6</b>	Gas pressure evolution of bentonite suspensions with VGH at 120.33 ± 0.04 °C. Headspace volume in the vessels with suspensions was adjusted to 3.3, 6.6 and 13.2 cm <sup>3</sup> by varying the VGH volume.....	24

<b>Fig. 3.7</b>	Gas pressure evolution of Opalinus and COX (Bure) claystone 1:1 and 1:2 suspensions with OPA and COX at $90.5 \pm 0.2^\circ\text{C}$ . Headspace volume of the vessels was adjusted to $13.2 \text{ cm}^3$ .....	25
<b>Fig. 3.8</b>	pH of VGH and OPA at the onset and after 1, 8, 30, $430 \pm 11$ , and 760 days of reaction with bentonites at $25^\circ\text{C}$ . Low volumes of supernatant OPA for SD80 precluded pH measurements after 8 days of reaction.....	26
<b>Fig. 3.9</b>	pH of VGH after reaction with bentonites for 760 days at $25^\circ\text{C}$ , $355 \pm 5$ days at $90^\circ\text{C}$ , 690 days at $90^\circ\text{C}$ , and 385 days at $120^\circ\text{C}$ .....	27
<b>Fig. 3.10</b>	pH of VGH after reaction with bentonites at $90^\circ\text{C}$ for 355 days plotted against the pH differences between VGH solutions after reaction with bentonites at $25^\circ\text{C}$ for 760 days and at $90^\circ\text{C}$ for 355 days.....	27
<b>Fig. 3.11</b>	pH plotted against Si concentration (mM) for VGH without (circles) and with substrate (diamonds) after one- and two-year reactions with bentonites at 25 and $90^\circ\text{C}$ .....	29
<b>Fig. 3.12</b>	(a) pH plotted against Si concentration for VGH after one-year reaction with bentonites at $120^\circ\text{C}$ , and (b) corresponding shifts of charge concentrations. Coefficient of determination $R^2$ for linear regression of data in graph b ( $\Delta n.c. = (0.20 \pm 0.11) \times \Delta p.c. + 41 \pm 24$ ) equals 0.20 .....	29
<b>Fig. 3.13</b>	Shifts of charge concentrations in VGH without (circles) and with substrate (diamonds) relative to unreacted VGH after one- and two-year reactions with bentonites at 25 and $90^\circ\text{C}$ .....	31
<b>Fig. 3.14</b>	Evolution of permeability for VGH ( $\text{m}^2$ ) of unreacted bentonites in the first series .....	34
<b>Fig. 3.15</b>	Evolution of permeability for VGH ( $\text{m}^2$ ) of unreacted bentonites (a) and bentonites reacted with VGH for $430 \pm 11$ days at $25^\circ\text{C}$ (b – d) in the second series.....	34
<b>Fig. 3.16</b>	Swelling pressure and solution uptake for unreacted B04 (a), B13 (b), B16 (c), and B31 (d) at respective dry densities of 1.52, 1.52, 1.54, and $1.57 \text{ g/cm}^3$ upon saturation with VGH (supplied by burettes connected to inlets at cell bottoms for 30 days and at cell tops afterwards). Insets show close-ups for the first four days of saturation ....	36

<b>Fig. 3.17</b>	Swelling pressure evolution for unreacted (a) B04, B13, B16, B19, and B31, and (b) B09, B11, B12, B36, and B37 at dry densities in the range 1.51 – 1.59 g/cm <sup>3</sup> upon saturation with VGH in the first series. VGH was supplied by burettes for 44 to 57 days and by a pump afterwards.....	37
<b>Fig. 3.18</b>	Swelling pressure evolution for (a) unreacted B10, B19, B38, B49, and SD80 at dry densities in the range 1.47 – 1.55 g/cm <sup>3</sup> , and (b) B04, B13, B19, B31, B38, and SD80 after reaction with VGH for 430 ± 11 days at 25 °C upon saturation with VGH in the second series. VGH was supplied by burettes for 75 days and by a pump afterwards.....	38
<b>Fig. 3.19</b>	Stress applied to compact B10, B38, B49, and SD80 to a density of 1.6 g/cm <sup>3</sup> in the first loading followed by an unloading and two further loadings/unloadings .....	38
<b>Fig. 4.1</b>	Changes of swelling pressures and permeabilities for bentonites upon a reaction with VGH for 430 ± 11 days at 25 °C .....	45
<b>Fig. 4.2</b>	Swelling pressures (top panel) and permeabilities (bottom panel) of bentonites reacted with VGH for 430 ± 11 days at 25 °C upon their changes with respect to those of unreacted bentonites.....	46
<b>Fig. A.1</b>	Fe(II) and Fe(III) contents in reference specimens measured by GRS and reported by CRPG and PNNL /AMO 98/ .....	61
<b>Fig. A.2</b>	Total Fe and Fe(II) contents in B36 before and after one- and two-year reactions with VGH and OPA. Initial contents in a) and c) are for un-washed B36, whereas those in b) and d) for washed B36 .....	62
<b>Fig. A.3</b>	Total Fe and Fe(II) contents in SD80 before and after one- and two-year reactions with VGH and OPA.....	63

## A Annex: Measurements of Fe(III)+Fe(II) and Fe(II)

A method using 1,10-phenanthroline to quantify Fe(II) and total Fe in bentonites /AMO 98/ using UV/VIS spectrometer 2450 (Shimadzu) was applied, which is based on a dissolution of constituting minerals with HF and H<sub>2</sub>SO<sub>4</sub> and allows a precise quantification of Fe(II) and total Fe in layer silicates /ANA 08/, /LIU 11/. Powdered geochemical reference specimens of a mica (Mica-Fe), a glauconite (GL-O) and a phlogopite obtained from the Centre de Recherches Petrographiques et Geochimiques (CRPG, <http://helium.cprg.cnrs-nancy.fr/SARM/pages/geostandards.html>) were analysed to confirm an appropriate implementation of the method (Fig. A.1). The lower boundary of calibrated Fe contents for Fe analyses was set to 1 wt%.

Results of the measurements of total Fe and Fe(II) in bentonites B36 (Fig. A.2) and SD80 (Fig. A.3) after reaction with VGH and OPA with/without substrate did not reveal a clear effect of possible activity of Fe(III)-reducing organisms at the studied experimental conditions. The results for bentonites after one-year reaction were obtained using a protocol engaging a separate subsample for estimation of water content of the subsamples digested for the determination of Fe contents and show a generally lower consistence with the initial total Fe contents. The protocol was optimized to measure the water content of subsamples before digesting them in the aftermath, which provided a better consistence with the initial total Fe contents of the results for bentonites after one-year reaction.

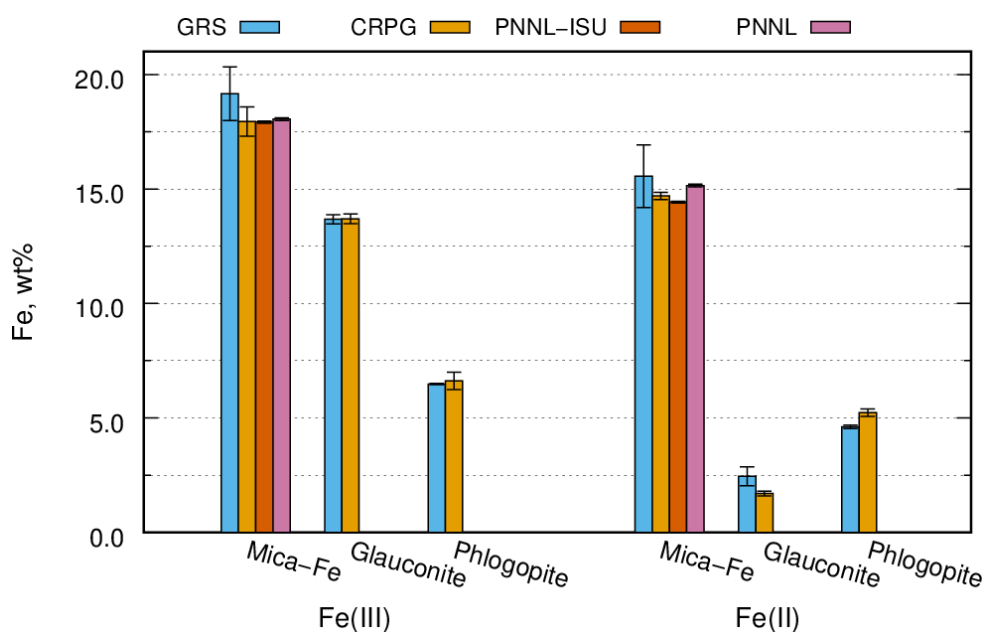


**Fig. A.1** Fe(II) and Fe(III) contents in reference specimens measured by GRS and reported by CRPG and PNNL /AMO 98/

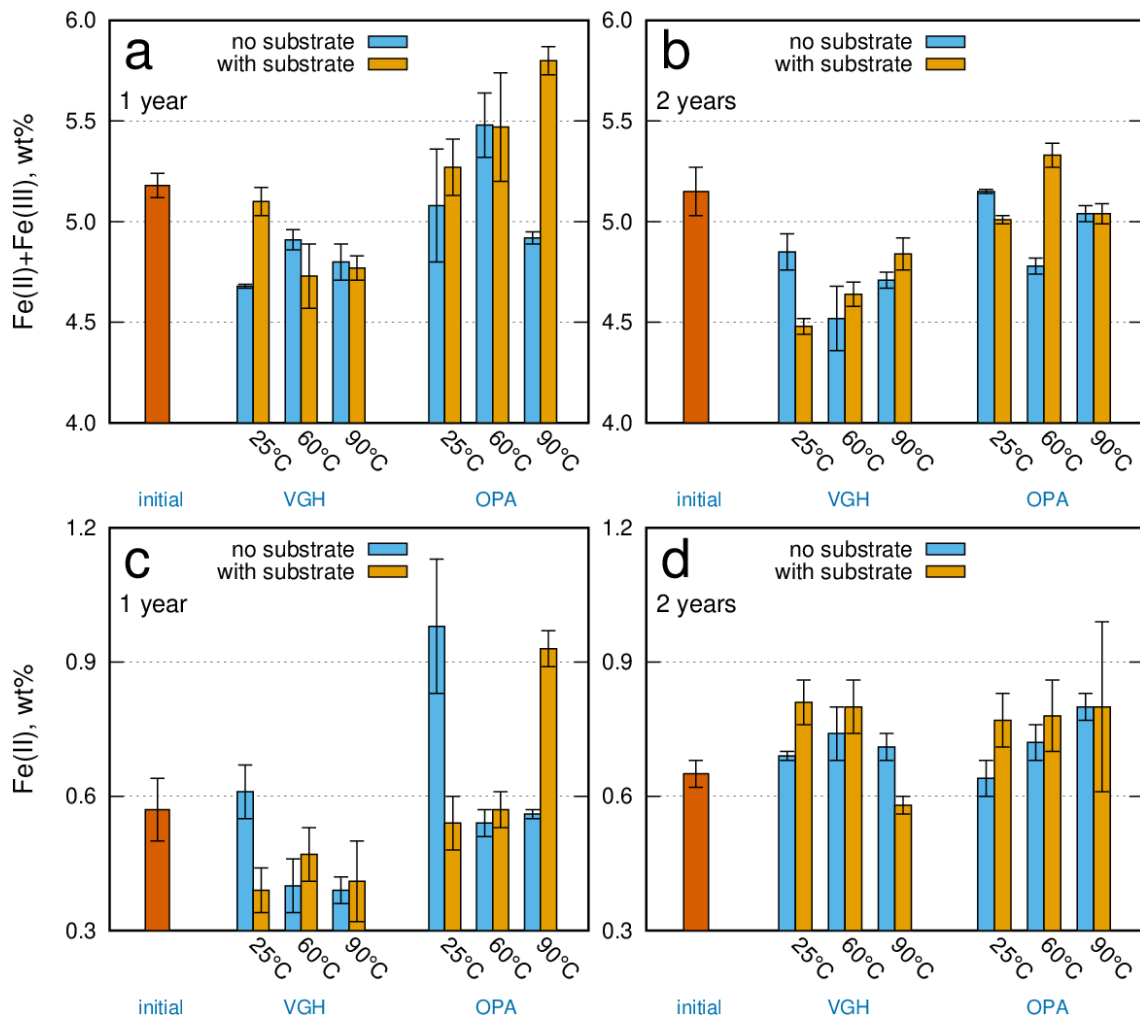


**Fig. A.2** Total Fe and Fe(II) contents in B36 before and after one- and two-year reactions with VGH and OPA. Initial contents in a) and c) are for unwashed B36, whereas those in b) and d) for washed B36

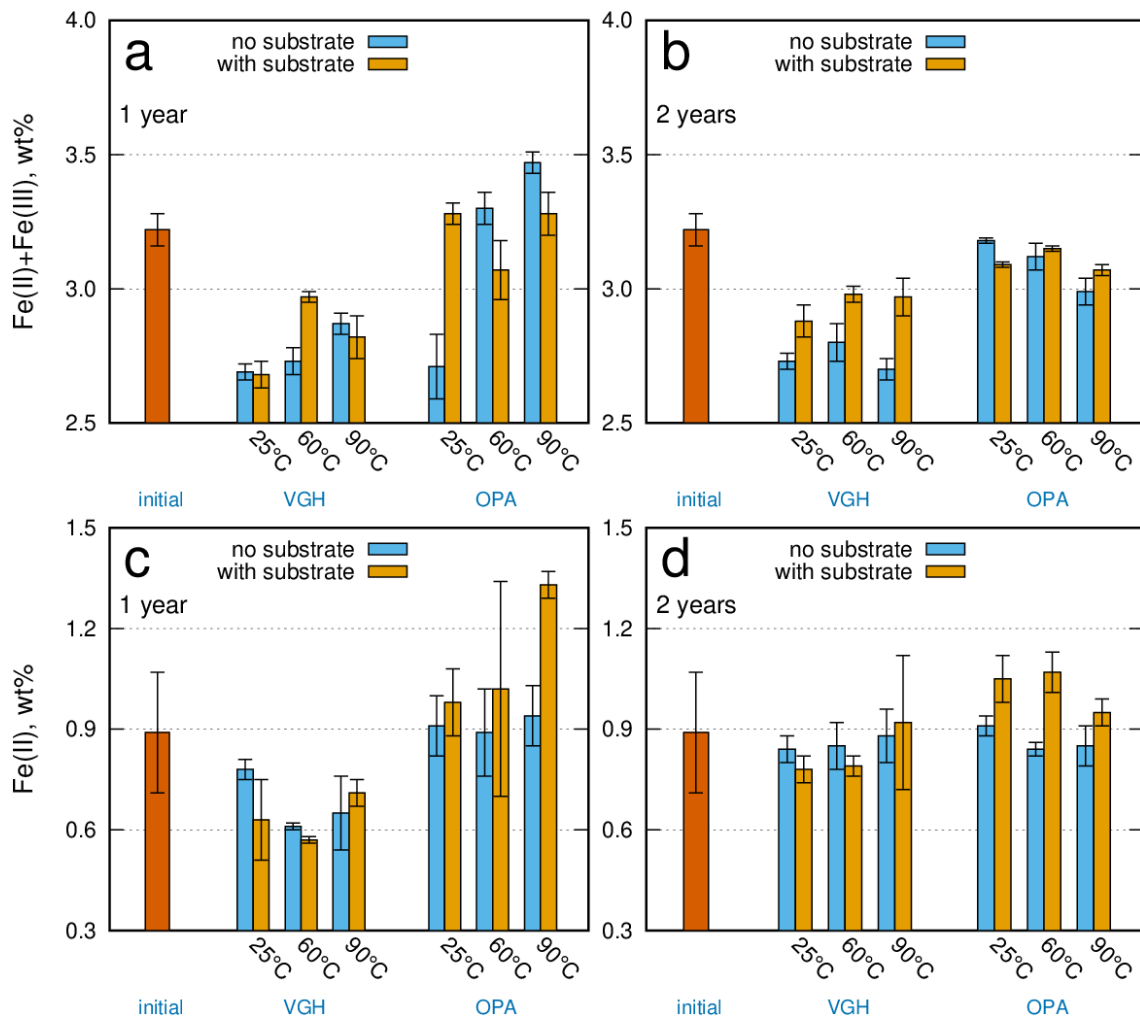


**Fig. A.3** Total Fe and Fe(II) contents in SD80 before and after one- and two-year reactions with VGH and OPA

**Gesellschaft für Anlagen-  
und Reaktorsicherheit  
(GRS) gGmbH**

Schwertnergasse 1  
**50667 Köln**  
Telefon +49 221 2068-0  
Telefax +49 221 2068-888

Boltzmannstraße 14  
**85748 Garching b. München**  
Telefon +49 89 32004-0  
Telefax +49 89 32004-300

Kurfürstendamm 200  
**10719 Berlin**  
Telefon +49 30 88589-0  
Telefax +49 30 88589-111

Theodor-Heuss-Straße 4  
**38122 Braunschweig**  
Telefon +49 531 8012-0  
Telefax +49 531 8012-200

[www.grs.de](http://www.grs.de)